Solid State Phenomena Vols. 85-86 (2002) pp. 353-414

Characterisation of Hydrogen and Hydrogen-Related Centres in Crystalline Silicon by Magnetic-Resonance Spectroscopy

C.A.J. Ammerlaan and P.T. Huy

Van der Waals-Zeeman Institute, University of Amsterdam, Valckenierstraat 65, NL-1018 XE Amsterdam, The Netherlands

Keywords: Hydrogen, Magnetic Resonance, Silicon

Abstract

In recent years research by magnetic resonance has contributed substantially to the understanding of hydrogen and hydrogen-related centres in crystalline silicon. As usual for magnetic resonance, which was applied in its varieties of electron paramagnetic resonance (EPR) and electron-nuclear double resonance (ENDOR), in several cases profound insight into the microscopic structure of centres has been the result of the studies. This includes atomic structure by identifying the chemical nature of impurity atoms and the symmetry of their geometrical arrangement within in the defect, as well as electronic structure by mapping of the defect-electron wave function. In this paper, research will be reviewed on centres which after hydrogen interaction are in a paramagnetic state. Hydrogen in its pure configuration of an isolated neutral atom on a bond-centred position in trigonal symmetry as the prototype of hydrogen centres, is described first. Shallow thermal donor centres formed at elevated temperature, similar to, but distinctly different from the more familiar oxygen-related thermal donors, are considered next. Several intrinsic lattice defects and impurities remain in a paramagnetic state, in cases when interaction with hydrogen does not lead to full passivation. Recent research on hydrogen binding on dangling bonds in mono- or multi-vacancies has resulted in the observation and understanding of several fundamental defect structures. Double donors, such as the thermal double donor and the substitutional chalcogen atoms sulphur an selenium, have been found to bind one hydrogen atom on several distinct positions remaining electrically active. Hydrogen interaction with impurities with deep electronic levels, more difficult to describe theoretically, has also been observed. In this category, transition elements from the iron, palladium and platinum groups are the examples which are considered. In an appendix the spectroscopic parameters of 32 magnetic resonance spectra with relation to hydrogen are summarised.

1. Introduction

Over the last twenty years the importance of hydrogen as a beneficial or detrimental impurity in semiconductors, in particular in silicon, has been recognised. Due to its small size and the open lattice of the diamond structure, the hydrogen atom or ion can easily penetrate the bulk of the material. The activation energy for migration is only 0.48 eV, which is among the lowest for impurities in silicon [1, 2]. Hydrogen can easily intentionally be introduced by diffusion [1, 3, 4], implantation [5 – 7], hydrogen plasma treatment [8], wet chemical etching [9, 10] or by boiling in water [11, 12]. Inadvertently, hydrogen is present, often unknown, as an impurity introduced during process steps in device manufacturing. Due to its half-filled 1s electronic shell the hydrogen atom has a high reactivity. A second electron can be accommodated in this shell with low energy. As a result hydrogen binds easily and strongly to defects with broken bonds or other centres which offer single valence electrons. For most centres, intrinsic lattice defects or chemical impurities, with shallow or deep electronic levels, this condition holds. For this reason hydrogen is involved in a rich variety of defect interactions. As these interactions may change the electronic properties of the material, in a stable or easily reversible fashion, this behaviour of hydrogen is of utmost relevance for materials applications. The passivation of shallow acceptors [13 – 15] and donors [16] is one of the more spectacular effects of hydrogen presence. Another most important application is the passivation of dangling bonds with the elimination of their associated electron traps or recombination centres in amorphous material, used, e.g., in solar cell production. Strongly motivated by the relevance for materials science, the more fundamental studies of the atomic and electronic structures of hydrogen-related centres have witnessed intensive activity since around 1985. As important as the passivation process may be for the materials properties, the direct observation of passivated products is by definition difficult. Passivated defects do not have electronic levels in the semiconductor band gap and are diamagnetic. The stable hydrogen molecule maybe is the most striking form of hydrogen presence to easily escape detection. For this reason several of the powerful experimental techniques for defect study fail. An outstanding technique for defect characterisation as electron paramagnetic resonance, requiring centres with non-zero spin, suffers from the handicap that passivated centres are not detectable. Nevertheless, in several cases the passivation by hydrogen bonding is not complete. For instance, this will happen for larger defects, such as multi-vacancies and interstitial complexes. In the category of double donors and acceptors the binding of one hydrogen atom may lead to partial passivation, with the possible consequence of the conversion of a double dopant into a single dopant. For transition elements with in many cases a high value of electron spin, the binding of a hydrogen atom will not render them diamagnetic. Even, as an opposite effect, the binding of hydrogen can activate a centre, such as the iso-electronic impurity carbon [9, 17]. Altogether, a vast field for fruitful studies is still left open. As a result, continued efforts with magnetic resonance over the last 15 years have seen a number of successful investigations. In this report a review is given, sometimes brief, of the main results obtained. Materials properties and phenomena related to hydrogen in semiconductors are covered by several review papers and books; a list of such publications is included in the section references.

2. Isolated hydrogen

No doubt, the most prominent magnetic resonance spectrum related to hydrogen in silicon is spectrum Si-AA9 [18, 19]. The spectrum was produced both in float-zoned and Czochralski-grown silicon by hydrogen implantation in the energy range of 7–30 MeV in a spatially homogeneous distribution, at the temperature of 80 K. Samples received a thermal anneal at 195 K for 40 minutes. Illumination of the sample is required for observation of the spectrum. It has been identified as arising from a single neutral hydrogen atom on the bond-centred position between two silicon atoms. In Fig. 1 a typical EPR spectrum is shown. It was recorded in a spectrometer operating at the microwave frequency of 37.47 GHz, with the magnetic field parallel to a <100> crystal direction, at the temperature of 77 K. A most important feature in the spectrum is the splitting of the main line in two components of equal intensity. The structure is due to the hyperfine interaction with one nucleus of spin $I = 1/2$ and abundance of 100%, which must be identified as hydrogen. This constitutes the first direct evidence in an EPR spectrum of hydrogen presence. Certainly this observation in the Si-AA9 spectrum has been important stimulation for further application of magnetic resonance in the study of hydrogenation effects in silicon. Replacing the hydrogen atom by deuterium the number of hyperfine structure lines increases to three, but the splitting almost collapses [7]. This is consistent with the nuclear spin $I = 1$ of the deuteron and its smaller nuclear g factor, i.e., $g_d/g_p = 0.15$, providing confirmation of the hydrogen involvement. In the spectrum also hyperfine interaction with ^{29}Si nuclei of the host crystal is discernible. The positions of these resonances are indicated in Fig. 1. Their intensity is near 5% of the main line, which, given the 4.7% abundance of the ^{29}Si isotope and its nuclear spin $I = 1/2$, implies that two silicon atoms are present in the centre on symmetry-equivalent sites. Measuring the angular variation of the resonance fields, patterns revealing the trigonal symmetry for the EPR centre are obtained, for the fine structure of the electronic Zeeman effect as well as for the hyperfine interactions with hydrogen and silicon. This leads to the defect model as one hydrogen atom on a bond-centred position, midway between two nearest-neighbour silicon atoms. In this H_{BC} model the hydrogen atom occupies a site with inversion symmetry. The crystallographic point-group symmetry is thus established as $\bar{3}$m.

For the quantitative analysis of the spectroscopic information the spin Hamiltonian

$$H = \mu_B \boldsymbol{B}\cdot\boldsymbol{g}_e\cdot\boldsymbol{S} + \Sigma_j[-(\mu_j/I_j)\boldsymbol{B}\cdot\boldsymbol{I}_j + \boldsymbol{S}\cdot\boldsymbol{A}_j\cdot\boldsymbol{I}_j] \quad (1)$$

is appropriate, with index j indicating the magnetic nucleus (proton p, deuteron d, silicon ^{29}Si, or muon μ). Principal values of the tensors, parallel and perpendicular to the threefold rotation axis, are given in table 1 and in the Appendix. Substantial support to the model follows from studies of the anomalous muonium atom, Mu* or μ^+e^-, in silicon, which forms an analogue of the neutral hydrogen on the bond-centred site. On one hand, the muon can be considered as a light isotope, mass $m_\mu = 207.769m_e$, of hydrogen with $m_p = 1837.15m_e$; on the other hand, as a lepton, it has $g_\mu =$

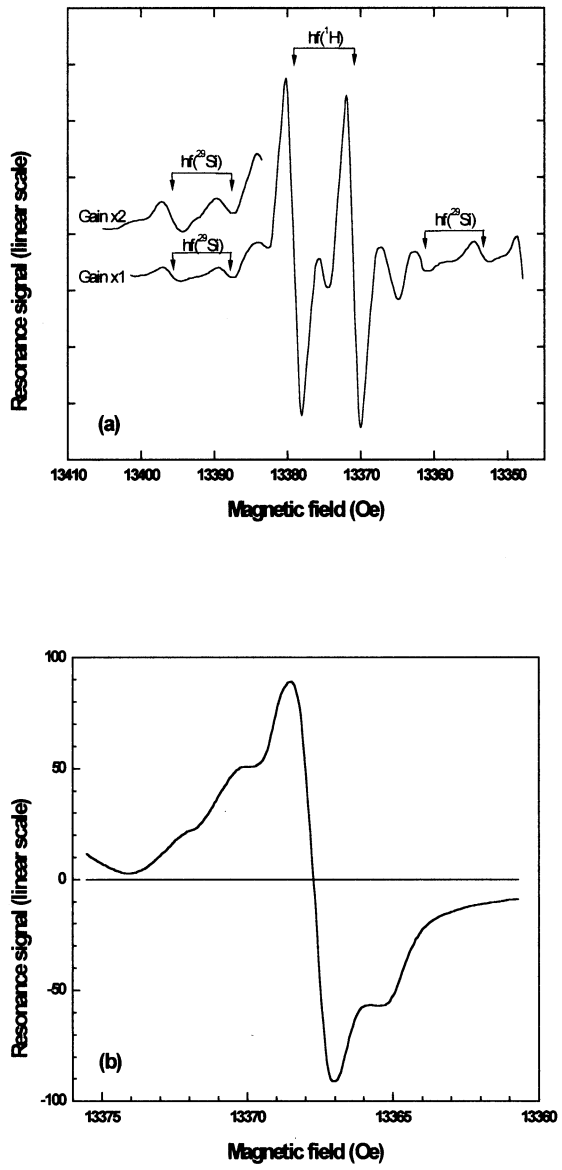

Fig. 1. Electron paramagnetic resonance spectrum of the Si-AA9 centre observed in hydrogen-implanted silicon. Observation conditions: sample illumination, temperature 77 K, magnetic field parallel to <100>, microwave frequency 37.47 GHz. (a) Hyperfine interactions with ^{1}H and ^{29}Si are indicated by the arrows, (b) hyperfine structure in deuterium-implanted silicon. After Gorelkinskii and Nevinnyi [19].

Table 1. Hyperfine parameters, from EPR and μSR experiments and from spin-density functional theory, for the centre $(H_{BC})^0$ and anomalous muonium, Mu*, together with coefficients η^2, α^2 and β^2 from LCAO analysis.

Centre	Nucleus	$A_{//}$ (MHz)	$A_\perp$ (MHz)	a (MHz)	b (MHz)	η^2	α^2	β^2	Method	Reference
$(H_{BC})^0$	^{1}H	–6.2	–31.4	–23.0	8.4				EPR	7
Mu*	Mu	–16.82	–92.59	–67.33	25.26				μSR	20
Mu*	Mu	9.6	–57.3	–35	22.3				theory	21
$(H_{BC})^0$	^{29}Si	–139.0	–72.9	–94.9	–22.0	0.24	0.095	0.905	EPR	7
Mu*	^{29}Si	–137.5	–73.96	–95.1	–21.2	0.23	0.099	0.901	μSR	22
Mu*	^{29}Si	–128	–63.5	–85	–21.5	0.22	0.09	0.91	theory	21

2.0016 ≈ 2. The muon spin rotation (μSR) method allows the determination of the hyperfine interactions with muon and silicon nuclei [20, 22]. Results, included in table 1, directly show that the hyperfine interactions with the ^{29}Si neighbour nuclei are almost identical in Mu* and $(H_{BC})^0$. On comparing the hyperfine interactions with the proton in $(H_{BC})^0$ and the muon in Mu* one finds a_μ/a_p = 2.93 and b_μ/b_p = 3.01. This matches quite well with the ratio of the magnetic moments of muon and proton: $\mu_\mu/\mu_p = (g_\mu/m_\mu)/(g_p/m_p)$ = 3.17. It may be concluded from these EPR results on the Si-AA9 centre and the data for Mu* obtained by μSR that the structures of the two centres are equivalent. Also included in table 1 are theoretical data based on first-principles calculations of the hyperfine interactions [21]. The agreement with data from experiment is satisfactory and in particular the signs of the interactions, positive or negative, are given by the theory, allowing adjustment of experimental results.

To these hyperfine coupling strengths the usual analysis based on a wave function constructed as a linear combination of atomic orbitals (LCAO) can be applied. With restriction to the hydrogen atom and its two neighbouring silicon atoms the wave function is given by

$$\psi = \eta_H(\alpha_H\varphi_{Hs} + \beta_H\varphi_{Hp}) + \eta_{Si}(\alpha_{Si}\varphi_{Si3s,1} + \beta_{Si}\varphi_{Si3p,1}) \pm \eta_{Si}(\alpha_{Si}\varphi_{Si3s,2} + \beta_{Si}\varphi_{Si3p,2}), \quad (2)$$

with wave functions on the atoms normalised by $\alpha_j^2 + \beta_j^2 = 1$. The isotropic parts a and anisotropic

parts b of the hyperfine interactions are related to the s- and p-type wave functions, respectively, by

$$a_j = (2/3)\mu_0 g_e \mu_B g_n \mu_n \eta_j^2 \alpha_j^2 |\varphi_{js}(r_j=0)|^2 \quad (3)$$

and

$$b_j = (2/5)(\mu_0/4\pi) g_e \mu_B g_n \mu_n \eta_j^2 \beta_j^2 \langle r_{jp}^{-3} \rangle. \quad (4)$$

For the two silicon atoms the analysis is straightforward. With a = –94.9 MHz and b = –22.0 MHz, and using the atomic parameters $|\varphi_{Si3s}(r=0)|^2 = 31.5\times10^{30}$ m^{-3} and $\langle r_{Si3p}^{-3} \rangle = 16.1\times10^{30}$ m^{-3} [23], one obtains $\eta_{Si}^2 = 0.24$, $\alpha_{Si}^2 = 0.095$ and $\beta_{Si}^2 = 0.905$. Considerable spin density is thus localised on the two nearest-neighbour silicon atoms in orbitals of strong p-type nature. Analysis of the hyperfine interaction with the hydrogen nucleus is more complex, as is immediately obvious from the negative sign of the isotropic parameter a, opposite to the sign of b, which is at variance with Eqs (3) and (4). Appreciable admixture of hydrogen p orbitals, as included in Eq. (2), is highly unlikely as the corresponding states are high in energy. In Eq. (2) one must have $\beta_H \approx 0$. The anisotropy in the hyperfine interaction is induced by remote spin density, in particular that on the silicon neighbour atoms. Accepting a point spin-density distribution on these two atoms, the anisotropy parameter b can be calculated from the equation

$$b = (\mu_0/4\pi) g_e \mu_B g_p \mu_n \eta_{Si}^2 R^{-3}. \quad (5)$$

With the calculated $\eta_{Si}^2 = 0.24$ on each atom and the observed b = 8.4 MHz the required distance between hydrogen atom and silicon neighbour is found as R = 0.165 nm. In the rigid lattice the hydrogen inserted on the BC site is at the distance of 0.118 nm from the silicon neighbours. The slightly increased value found for the distance is consistent with the established outward relaxation of the silicon atoms, theoretically calculated as being 0.041 nm [24] or 0.045 nm [25] and here experimentally determined as 0.047 nm, and the enhanced p-type character of the orbital. In this description the spin density is localised on the silicon atoms without a lobe pointing preferentially inwards towards the hydrogen atom. Such an assumption is consistent with the anti-bonding nature as regards the silicon orbitals. A one-electron LCAO diagram, as given by Figs 2(a,b), shows the hydrogen atom on the site of the inversion centre. The orbital belongs to the a_{1u} irreducible representation in the point group $\bar{3}$m. For the hydrogen an isotropic hyperfine interaction with a = –23 MHz is measured. In the LCAO analysis, using the Eqs (2) and (3) and ignoring the problem of the minus sign, this results in $(\eta_H)^2 = 0.016$. Although the calculated localisation is small, it is inconsistent with the a_{1u} symmetry type of the orbital carrying the unpaired spin requiring a node at the hydrogen site. A solution towards this problem is provided by considering all three electrons in the system. In the more-electron description the ground state has wave function $\psi = (a'_{1g})^+(a'_{1g})^-(a_{1u})^+$, where superscripts + and – indicate the two spin states, $a'_{1g} = [\varphi_{Hs} + (1/2)\lambda\sqrt{2}(\sigma_{Si1} + \sigma_{Si2})]/$

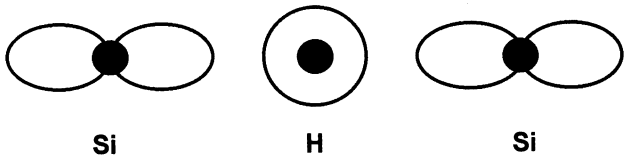

(a)

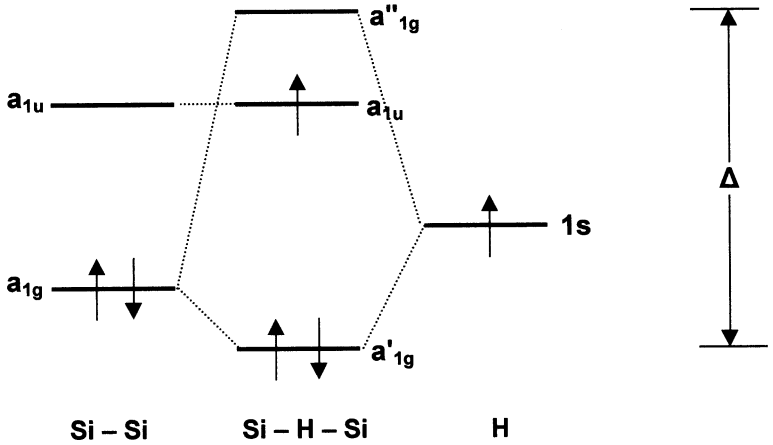

(b)

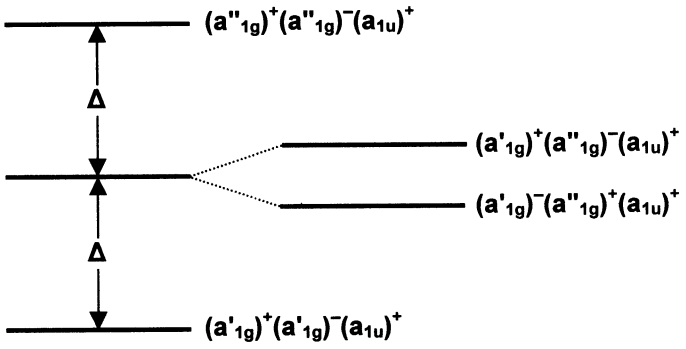

(c)

Fig. 2. Bonds and energy levels for the neutral Si-H-Si molecule, (a) H in a bond-centred Si-Si position, (b) a one-electron tight-binding model, after Van de Walle [31], (c) energies and wave functions in a three-electron model.

$(1 + \lambda^2)^{1/2}$ and $a_{1u} = (1/2)\sqrt{2}(\sigma_{Si1} - \sigma_{Si2})$. Spin density on the hydrogen atom arises from polarisation of the electrons in the 1s core states. In a second mechanism, spin density can follow from configuration interaction with excited states. Within the LCAO model three excited states with the a_{1u} symmetry have wave functions $(a'_{1g})^+(a''_{1g})^-(a_{1u})^+$, $(a'_{1g})^-(a''_{1g})^+(a_{1u})^+$ and $(a''_{1g})^+(a''_{1g})^-(a_{1u})^+$, with $a''_{1g} = [\lambda\varphi_{Hs} - (1/2)\sqrt{2}(\sigma_{Si1} + \sigma_{Si2})]/(1 + \lambda^2)^{1/2}$. Energies, as indicated in Fig. 2(c), of the first two states are equal to first order, but the level is split by correlation effects. Their different admixture into the ground state leads to spin density on the hydrogen atom.

Several other important features of the single hydrogen centre in silicon have been studied by magnetic resonance. This includes defect alignment induced by uniaxial stress and thermal relaxation [26], isochronal thermal annealing in dark conditions of $(H_{BC})^+$ in the temperature range 190–220 K and of the Si-AA9 spectrum of $(H_{BC})^0$ under illumination between 110 and 130 K [19, 27 – 29], the stable positions of H^+ and H^0 on the bond-centred site versus the position of H^- on the tetrahedral interstitial site [24, 30, 31], together with the negative-U character of the donor and acceptor levels rendering the neutral charge state unstable [25, 32, 33]. For further discussion, reference is made to the literature [7].

3. Hydrogen-related donor centre

It has been frequently observed that shallow donor centres in silicon are created by irradiation when hydrogen is present. The presence of hydrogen can either be a hydrogen atmosphere, gas or plasma, during a particle irradiation, such as neutrons, or the direct hydrogen implantation. In the latter situation, typical conditions are proton implantation at room temperature in the energy range of several MeV, followed by thermal anneal in the range of 300 to 500 °C for some tens of minutes. Up to the implantation dose of 10^{17} H/cm^2 the donor formation was found to be proportional to dose [7]. The donor centres are localised near the end of the range of the implanted particles where most of the lattice damage is created [34]. They are formed in float-zoned silicon and also, but to lower concentration, in crucible-grown silicon. Implantation of deuterons also generates the donor centres, but following helium implantation under similar conditions they are not observed [34, 35]. Guided by these experimental facts one tends to conclude that hydrogen is an essential constituent of the donor centres, whereas other impurities, in particular oxygen, are not involved. This is suggestive for the formation of donors which are some complex of intrinsic crystal defects together with hydrogen. Thermal anneal above 600 °C destroys the donor centres. Donors formed under these conditions were observed by electrical conductivity [36], Hall effect [37], photo-thermal ionisation spectroscopy (PTIS) [38, 39] and by electron paramagnetic resonance [7, 19, 34]. Analysis of the Hall effect data reveals two donor levels, a shallow one at 35 meV and a deeper one at 160 meV below the conduction band [37]. By PTIS actually three shallow levels, HD4, HD5 and HD6, close together in energy were reported [39]. In EPR two centres related to the donors were observed. One of these, labelled HSD, is an isotropic resonance, when measured at X-band frequencies, consisting

of a single line without any resolved structure and with the g value g = 1.9987 [19, 34]. However, when recorded in K band, at the microwave frequency 23 GHz, with magnetic field $\boldsymbol{B}$ // <100>, the HSD resonance, as shown in Fig. 5, is split into two components with a 2:1 intensity ratio [7]. This demonstrates a slight anisotropy of the HSD resonance, which happens to be equal both in average g value and in the splitting to the reported g tensor of the oxygen-related orthorhombic spectrum Si-NL10 [40]. Resonance HSD has been described as arising from free conduction electrons attributed to ionisation of hydrogen-associated shallow donors (HSD). Observation of the spectrum requires temperatures above 30 K. At lower temperature the resonance disappears indicating a donor which is diamagnetic, S = 0, in the neutral state [19]. The HSD resonance is more typically observed after higher temperature annealing. For shorter anneal times or at lower temperatures a spectrum labelled Si-AA1 is observed. The two resonances represent the two members of a defect bistability system [36, 37]. A reversible conversion related to an atomic rearrangement process between the two structures can take place where the AA1 centre is formed when equilibrating the system at lower anneal temperatures around 100 °C and the isotropic HSD resonance prevails after high-temperature treatment near 300 °C [19]. The AA1 resonance is described by a single electron spin S = 1/2 and has no discernible hyperfine structure. From the angular variation of the resonance fields the symmetry is established as orthorhombic-I. Illumination is required for the observation indicating that the centre is observed under ionised conditions. It is interpreted as arising from the positive charge state of a hydrogen-related double donor, labelled HDD^+. The parameters of the Si-AA1 resonance demonstrate a close similarity with the Si-NL8 spectrum arising from ionised oxygen-related thermal double donors (TDD^+). Both spectra belong to S = 1/2 centres with the orthorhombic-I symmetry, point group C_{2v}, and the principal values of the g tensor are nearly equal [40 – 42]. Fig. 3 demonstrates this similarity. Both centres are formed as heat-treatment centres in the 300–450 °C temperature range and are related to double donors with similar first and second ionisation energies. Other evidence, however, indicates clear differences between the two centres. Production conditions are centre specific, NL8 requiring the presence of oxygen, AA1 requiring hydrogen. For the NL8 spectrum a series of defects with gradually decreasing donor ionisation energy with prolongation of the heat-treatment time exists, supported by unambiguous evidence from infrared optical absorption and magnetic resonance. For the AA1 spectrum no such separate components were distinguished in the EPR at Q-band frequencies near 37 GHz. More recently it was found that the two centres undergo a quite different alignment effect under conditions of externally applied stress [42, 43]. Their piezo-elastic tensors have a different sign for particular stress directions indicating that the two centres create different strains in the lattice. Also the relaxation after removal of the stress towards random alignment of defect orientations gives very different time constants. From Fig. 4 it can be noted that the AA1 centre reorients much faster than NL8. Nevertheless, the striking parallel between the hydrogen-related centres AA1 and HSD on one hand, and the oxygen-related NL8 and NL10 centres on the other hand, requires further clarification. Final atomic models for the centres HSD and AA1 are not available. The suggestion of a self-interstitial complex as a core to which either hydrogen or oxygen is attached has frequently

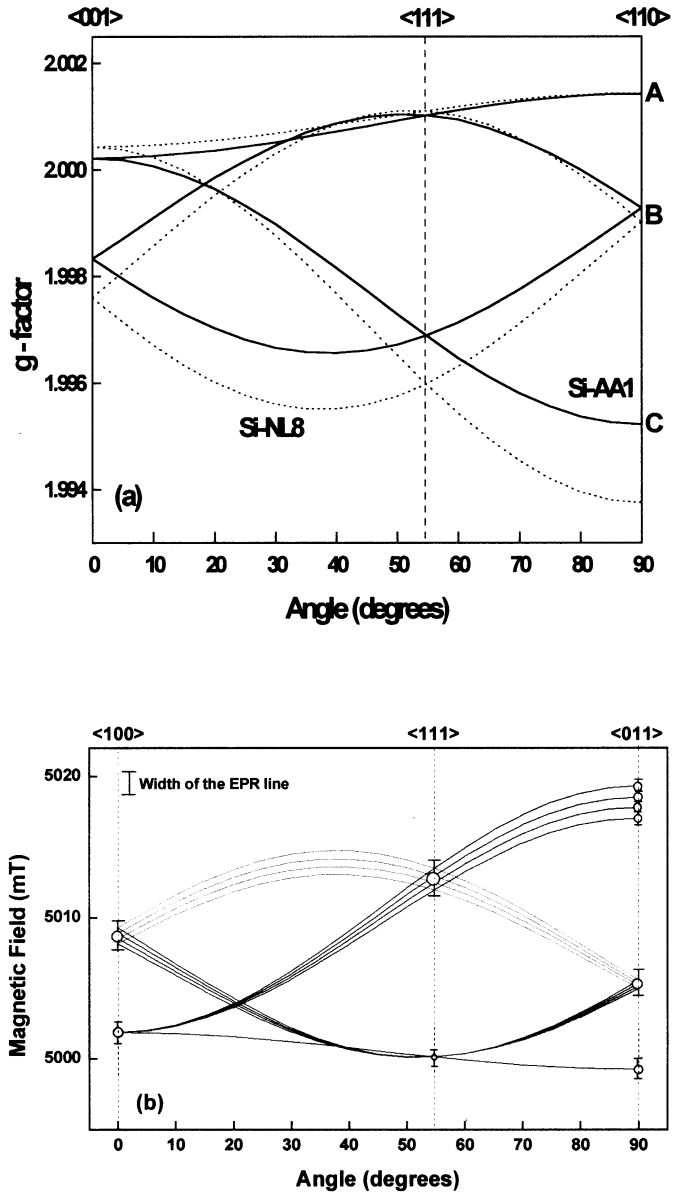

Fig. 3. (a) Angular dependence of the effective g values for the orthorhombic spectra Si-AA1 (solid lines) and Si-NL8 (dashed lines) for rotation of the magnetic field in the <0 $\bar{1}$ 1> plane. Q-band (35 GHz) data for Si-AA1 from Gorelkinskii, *et al.* [42], K-band (23 GHz) data for Si-NL8 from Muller, *et al.* [40]. (b) High-resolution measurements performed in D-band (140 GHz) for Si-NL8 are for the individual species Si-NL8(#1) to Si-NL8(#4) [41].

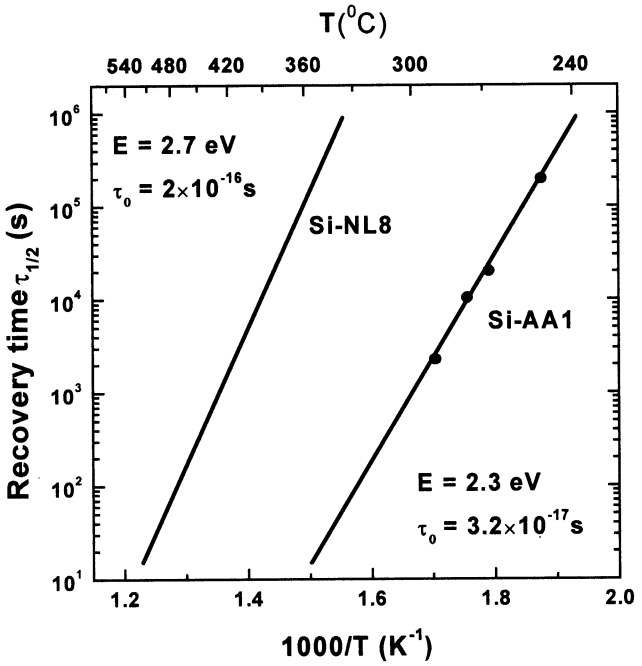

Fig. 4. Recovery time $\tau_{1/2}$ of the atomic reorientation for the Si-AA1 and Si-NL8 centres as a function of the temperature. After Gorelkinskii, *et al.* [42].

been made and provides a basis for understanding observed phenomena.

Upon thermal annealing of the samples at higher temperatures, in the range 350–550 °C, the intensity of the HSD signal decreases considerably. At the same time, a spectrum labelled Si-NL51 becomes observable. A spectrum recorded in K band, under conditions where both HSD and NL51 exist, is shown in Fig. 5. Identical spectra are produced by hydrogen and deuterium implantation. No structure due to hyperfine interaction is visible. Spectrum Si-NL51 has been observed both at X-band and K-band frequencies [44]. From the analysis it is concluded that its electron spin $S = 1$ and a zero-field splitting term $S{\cdot}D{\cdot}S$ is included in the spin Hamiltonian. As the spectrum is only observed under illumination of the sample by band-gap light it may arise from an excited triplet state of a neutral double donor. The angular dependence of resonance fields reveals the tetragonal symmetry for the defect, with $g_{//[100]} = 2.0071$ and $g_{\perp[100]} = 2.0007$. One of the few other centres in silicon with tetragonal symmetry, the neutron-irradiation defect Si-B3 [45], is simultaneously present. This is suggestive for a similar structure of the NL51 and B3 centres. The latter one has been identified as a <100>-split silicon di-interstitial in the positive charge state [46].

Several other EPR spectra have been observed after hydrogen implantation and thermal anneal. In Fig. 6 an overview is given of the temperature ranges of stability of these centres [19]. Their EPR

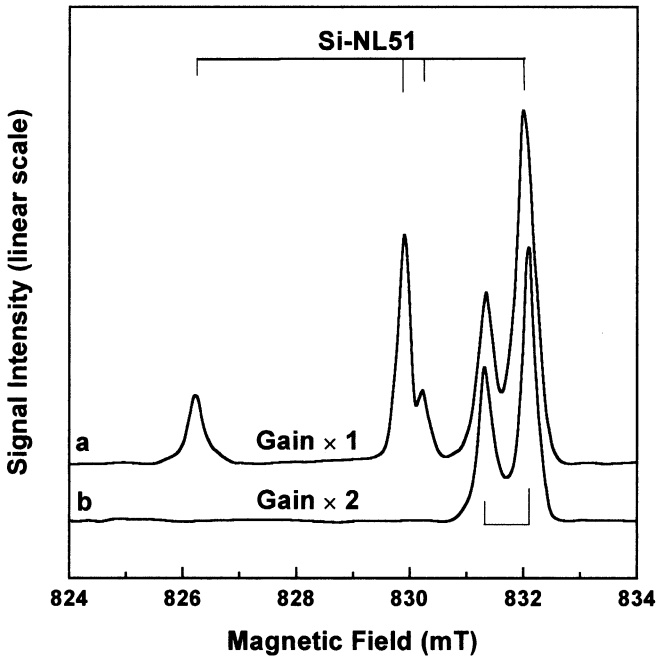

Fig. 5. EPR spectra of the Si-NL51 and HSD centres for $\boldsymbol{B}$ // <100>, microwave frequency 23.268 GHz. The NL10-like splitting of the HSD resonance is apparent. From Ref. 7.

parameters are summarised in the Appendix. Spectrum Si-AA10, corresponding to a centre of monoclinic symmetry is created in Czochralski silicon, and disappears around 180 K in 15-minutes isochronal anneal [18]. Spectrum S1 is prominently present after room-temperature hydrogen implantation. Observation under the high resolution of Q-band EPR revealed that spectrum S1 has components of trigonal and monoclinic symmetry [19]. The spectrum has recently been investigated in detail as will be discussed in the next section. Following anneal at higher temperatures the spectra AA2 and AA3, both from centres with the low triclinic symmetry, appear [19, 47, 48]. They correspond to centres of a more complex structure; for AA2 the model of a multi-vacancy cluster with a trapped hydrogen has been proposed. Most of these centres have not been thoroughly studied yet and consequently their modelling is far from established. Except for spectrum S1, in none of these spectra the presence of hydrogen is directly demonstrated by resolved hyperfine interactions with proton or deuteron. The conclusion towards hydrogen involvement in these centres is based on the more circumstantial evidence of production conditions. Although this may seem to form a weaker basis, it should be noted that the mentioned spectra are consistently observed when hydrogen or deuterium is implanted and are absent following implantation or irradiation with other particles. Hydrogen appears to be an essential requisite for formation.

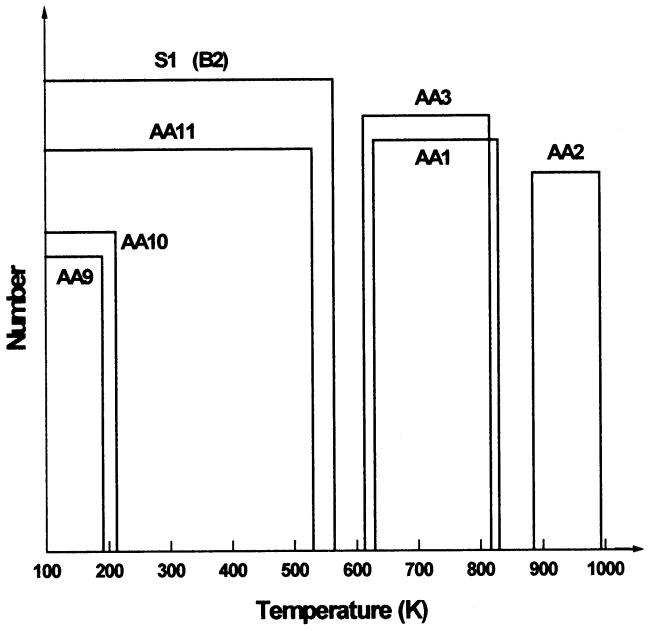

Fig. 6. The temperature ranges of stability of hydrogen-related EPR centres in proton-implanted silicon. After Gorelkinskii and Nevinnyi [19].

4. Hydrogen–vacancy centres

As early as 1967 the S1 EPR spectrum was observed, following 3 MeV proton irradiation at room temperature and absent after neutron irradiation, for which production conditions required the presence of hydrogen [5, 49, 50]. The production was proportional to implantation dose. The spectrum corresponds to centres produced along the proton track with increasing density towards the end of the particle range. In a 10-minutes isochronal anneal study the centres annealed out at temperatures in the range 200–300 °C. Spin-Hamiltonian parameters for the <111> axial defect are $S = 1/2$, $g_{//} = 2.0010$, $g_{\perp} = 2.0103$. In the higher resolution offered by Q-band EPR it was later discovered that the S1 centre actually is composed of several components, up to 5 in Czochralski silicon, with either the trigonal or the monoclinic-I symmetry [19, 51]. Only recently the centres were unambiguously identified as hydrogen related and their structure was unravelled in great detail. In this more recent literature the components of the S1 group of spectra are now labelled as VH^0, $S1_a$ and $S1_b$ [6, 52]. Another spectrum, Si-B2, is very similar to Si-S1. Both spectra belong to $S = 1/2$ centres with the trigonal symmetry, have equal g tensors within error limits, and equal temperatures for loss of spectra by thermal anneal, near 300 °C. It has therefore often be assumed

that the two spectra are in fact identical. It is, however, to be noted that in the original paper the spectrum B2 has been observed after N^+ and P^+ implantation [53] and in a later independent dedicated study also as the result of He^+, B^+, C^+ and N^+ implantation and neutron irradiation [54]. In this latter case any specific evidence for hydrogen presence was absent. This should leave open the possibility that B2 and S1 are different, maybe quite similar, centres with accidentally the same characterisation parameters. As another option, in view of the established frequent presence of hydrogen in nominally pure silicon crystals, the possibility that samples were unintentionally contaminated with hydrogen is open as well.

Production conditions and features of the spectra led to their identification as vacancy-type defects with hydrogen saturating a dangling bond [19]. In the most recent research the detailed models for the S1 centres were established. Spectrum VH^0 is related to a mono-vacancy with one of its four dangling bonds saturated by a hydrogen atom. The centre undergoes a Jahn-Teller distortion resulting in monoclinic-I symmetry, point group C_{1h}, or m, as observed at low temperatures, below 45 K. In this case the presence of the one hydrogen atom is established by just resolved hyperfine interaction. The deuterium hyperfine splitting, which will be around 6.5 times smaller, remains unobservable as it is smaller than the line width. In agreement with the model a strong hyperfine interaction is present with a unique silicon atom, isotope ^{29}Si. At higher temperatures a motional effect sets in related to electron switching between bonds, resulting in an apparent trigonal symmetry of the centre, as observed when measuring the spectrum above 110 K. The transition in the temperature range of interest is illustrated in Fig. 7 by spectra taken for $\boldsymbol{B}$ // <111>. The low-temperature monoclinic spectrum has the lines labelled A, B and C. The C line corresponds to centres with their Si-H axis parallel to the magnetic field direction. Their position does not change when the electron hops between the dangling or extended bonds of the other three silicon atoms. Lines A and B correspond to defect orientations which are inequivalent with respect to the magnetic field. With fast bond switching present, the resonance field will move to the weighted average of the original frozen positions. This will be at position AB = (2A + B)/3. The process can be followed in Fig. 7 for the temperatures spanning the range 45 to 225 K in which the transition takes place. The activation energy for the electron jump process is determined as E_a = 0.06 eV. Such a value is equal to the one measured for the same process in the phosphorus–vacancy complex (E centre) with its EPR spectrum Si-G8 [23]. This agrees with expectations as the atomic and electronic structure models for VH^0 and VP^0 have much in common. Spin-Hamiltonian parameters of the VH^0 centre are given in the Appendix.

In the same way as discussed for the AA9 centre, an LCAO analysis will yield a mapping of the electron spin distribution. For the single silicon atom, with the observed hyperfine principal values $A_{//}$ = –435 MHz and $A_\perp$ = –275 MHz, corresponding with isotropic value $a = (A_{//} + 2A_\perp)/3$ = –328 MHz and anisotropic part $b = (A_{//} - A_\perp)/3$ = –53 MHz, one obtains, using Eqs (3) and (4), η^2 = 0.60, α^2 = 0.13 and β^2 = 0.87. A comparison with the corresponding numbers for the VP^0 centre, η^2 = 0.59, α^2 = 0.14 and β^2 = 0.86 [23], confirms the close similarity of the two defects. From the large s-type hyperfine interaction on the silicon atom one concludes that the wave function has the

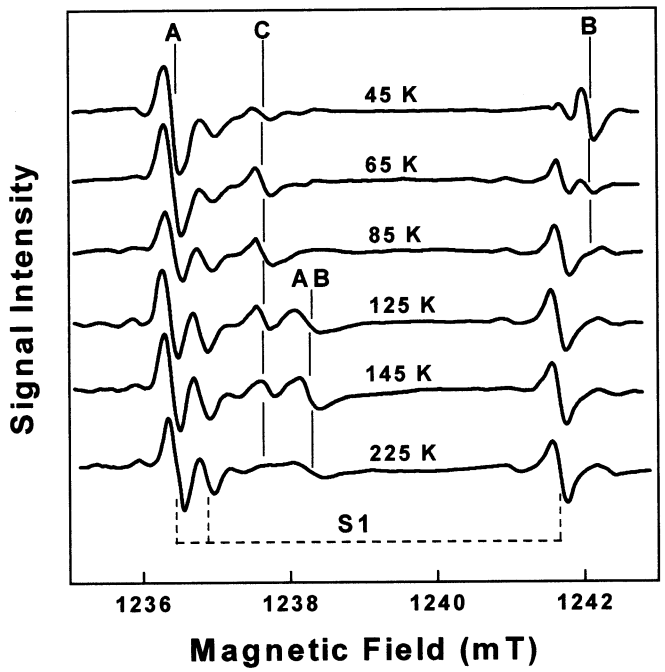

Fig. 7: Spectrum of VH^0 at different sample temperatures illustrating the transition from the low-temperature monoclinic-I structure at $T = 45$ K to the motionally averaged trigonal symmetry at $T = 145$ K. At $T = 225$ K the S1 resonances $S1_a$ and $S1_b$ dominate the spectrum. Microwave frequency 34.778 GHz, magnetic field $\boldsymbol{B}$ // [111]. After Bech Nielsen, *et al.* [52].

A_g symmetry type. The very small isotropic part of the hyperfine interaction with the hydrogen atom, $a = 0.2$ MHz, indicated that no s-type spin density is located on the hydrogen. In contrast to the similar situation for centre AA9 one can, however, not conclude that the hydrogen is located on a mirror plane with a node for the wave function. The low spin density is the result of the strong Si–H bond accommodating two electrons with opposite spin. As before for the AA9 centre, the LCAO analysis does not include anisotropic orbitals on the hydrogen site. The anisotropic part of the hyperfine interaction, $b = (-A_1 - A_2 + 2A_3)/6 = 4.15$ MHz, has to arise from distant spin density. The unpaired spin on the unique silicon atom can fully account for this interaction for $\eta^2 = 1$ and $R = 0.27$ nm. With a Si–H bond length of 0.148 nm this fits perfectly in an undistorted vacancy model where this distance is 0.28 nm. In a di-vacancy model the distance in the undistorted lattice amounts to 0.47 nm, which is far too big. It confirms the compact model of a mono-vacancy centre. Taking $\eta^2 = 0.60$, following the result of the silicon LCAO analysis, the required distance to the silicon atom with the dangling bond becomes 0.22 nm. This shorter distance can correspond to inward distortion of the unique silicon atom.

Two more spectra belonging to the S1 group of spectra were observed following proton implantation at temperatures below 130 K. The two spectra, labelled $S1_a$ and $S1_b$, are single-electron centres with $S = 1/2$, correspond to centres with monoclinic-I, near trigonal, symmetry. The spin-Hamiltonian parameters, as given in the Appendix, are very similar to those of VH^0. They are therefore interpreted as multi-vacancy centres in which hydrogen binds to a dangling bond. The main spin density is in another dangling bond of the vacancy structure. Only for $S1_a$ a hydrogen hyperfine structure due to one proton is observable in the spectra; for $S1_b$ such structure is absent. The isotropic part of this hyperfine interaction, $a = 2.3$ MHz, is again very small, indicating low spin density on the hydrogen atom. The anisotropic part, $b = 0.77$ MHz, is explained by remote interaction with spin density on the dangling bond, which, using Eq. (5), should be at a distance $R = 0.47$ nm. This fits perfectly with the geometry of a hydrogen in an undistorted di-vacancy. The $S1_a$ defect is therefore identified as a V_2H centre in the paramagnetic neutral state. For $S1_b$ the model of a tri-vacancy centre with hydrogen, $(V_3H)^0$, is proposed, with the tetra-vacancy centre $(V_4H)^0$ as a possible alternative. In these larger centres, with $R = 0.65$ nm and $R = 0.84$ nm, respectively, the distant hyperfine interaction would be too small to give observable splitting in the $S1_b$ spectrum. Silicon hyperfine interactions were measured for several shells of the $(VH)^0$, $S1_a$ and $S1_b$ centres. They allowed a detailed mapping of the electron spin density in the defect and showed great similarity between the three centres, as reflected in the modelling. Both centres $S1_a$ and $S1_b$ anneal out at temperatures around 250 °C. Motional effects, as reported for $(VH)^0$, are not observed for the $S1_a$ and $S1_b$ centres.

Given the strength of the Si–H bond one may expect that vacancy centres with their several dangling bonds, if unreconstructed, can accommodate more than one hydrogen. Such expectations based on simple chemical bonding arguments are corroborated by modern self-consistent theoretical calculations for the mono-vacancy, which predict stability of VH_n complexes, with $n = 1 - 4$ [57]. Experimental evidence for such centres is based on local vibrational mode spectroscopy [58, 59] and on optical detection of magnetic resonance (ODMR) [55]. In the latter study hydrogen /deuterium plasma-treated silicon was electron irradiated. A magnetic resonance spectrum labelled HVH, was observed corresponding to an orthorhombic-I centre with electron spin $S = 1$. This is associated with a $(VH_2)^0$ centre, which due to complete pairing of electron spins is diamagnetic in its ground state. The excited spin triplet state is formed by the illumination inherent in the ODMR method. Hydrogen hyperfine interaction is not resolved but is manifest in the line shape of hydrogenated samples, which is absent in the case of deuteration. Parameters of the spin-Hamiltonian analysis are given in table 2 and in the Appendix. Applying the standard LCAO analysis, the spin density on the hydrogen is found to be a mere 0.9%; it is low, as usual, reflecting the full occupation of the Si–H bonds. The experimentally observed $S = 1$ triplet state is formed by spins mainly residing on the silicon bond formed by the two non-passivated atoms opposite to the hydrogen atoms in the vacancy; one finds the localisation $\eta^2 = 0.68$ for the two atoms together. Inspection of table 2 shows the near coincidence of the parameters for the HVH and SL1 spectra, the latter spectrum corresponding to the oxygen–vacancy complex (A centre), which is also

Table 2. Parameters of the Si-HVH and Si-SL1 spectra, ascribed to the orthorhombic-I centres $(VH_2)^0$ and OV*, respectively, observed in an excited spin triplet state with $S = 1$ [55, 56]. Hyperfine interactions A are for the ^{29}Si isotope of two silicon neighbour atoms.

Spectrum	Model	Principal values coupling tensors			Unit
Si-HVH	$(VH_2)^0$	$g_{[1,0,0]} = 2.002$	$g_{[0,1,1]} = 2.005$	$g_{[0,-1,1]} = 2.002$	
		$D_{[1,0,0]} = -348$	$D_{[0,1,1]} = -302$	$D_{[0,-1,1]} = 650$	MHz
		$A_{//[1,1,1]} = 220$	$A_{\perp[1,1,1]} = 114$		MHz
Si-SL1	OV*	$g_{[1,0,0]} = 2.0076$	$g_{[0,1,1]} = 2.0102$	$g_{[0,-1,1]} = 2.0058$	
		$D_{[1,0,0]} = -350$	$D_{[0,1,1]} = -307$	$D_{[0,-1,1]} = 657$	MHz
		$A_{//[1,1,1]} = 216$	$A_{\perp[1,1,1]} = 112$		MHz

observed in an excited $S = 1$ state [56]. In both centres two of the vacancy dangling bonds are saturated, by either two hydrogen atoms or one oxygen atom, the spin resides on an extended bond formed between the two remaining silicon atoms of the vacancy. In view of this similarity in the electronic structure of the VH_2 and VO centres such a close correspondence of parameters follows reasonable expectations. It builds on the similarity as observed for the $(VH)^0$ and $(VP)^0$ centres, as discussed earlier [52]. On the proper interpretation of the Si-HVH ODMR spectrum contradicting opinions have been expressed [60 – 62].

In oxygen-rich, Czochralski, silicon, the most prominent irradiation defect is the vacancy–oxygen centre, often referred to as the A centre. Its structure can be viewed as the single lattice vacancy in which one extended bond is replaced by an Si–O–Si unit in the (0,1,1) plane, while still an elongated bond is formed between the two remaining nearest-neighbour silicon atoms in the perpendicular (0,–1,1) plane. Hydrogen can break this latter bond, bind to one of the dangling bonds, leaving an unpaired spin on the other. The spectrum of this neutral VOH centre has been reported [63]. At temperatures below 180 K it was found to correspond to a stable monoclinic-I configuration of the defect. At higher temperatures, above 240 K, hydrogen jumps rapidly between two equivalent sites in the (0,–1,1) mirror plane of the defect resulting in a motionally averaged spectrum of the orthorhombic-I symmetry. The motional effect is conceptually similar to that of the vacancy in its pure form, as observed in the VH^0 spectrum, but is more restricted due to the existence of the Si–O–Si bond which stabilises the (0,1,1) mirror plane. Hyperfine interaction with the hydrogen atom has the small isotropic value $a = 4.7$ MHz, indicating a nearly vanishing electron-spin density on the proton. From the anisotropic part of the hyperfine interaction, $b = 5.2$

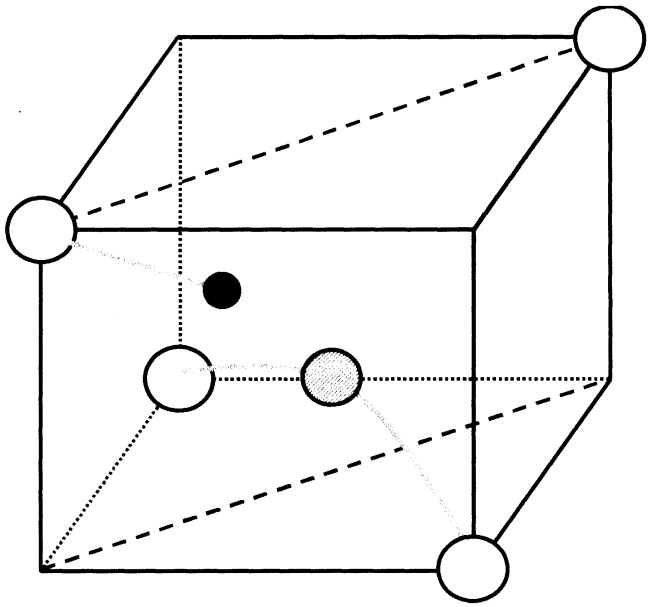

Fig. 8. Microscopic structure of the VOH complex, showing the position of the hydrogen atom (black) and the dangling bond in the (0,-1,1) mirror plane. The oxygen atom (hatched) is bonded to the two remaining nearest-neighbour silicon atoms in the (0,1,1) plane. After Johannesen, *et al.* [63].

MHz, the distance between hydrogen nuclear spin and electron is calculated as R = 0.25 nm, consistent with vacancy dimensions. An observed hydrogen/deuterium isotope effect confirms the defect model as illustrated in Fig. 8.

5. Hydrogen–thermal donor complexes

Research on thermal donors has a long history starting with the discovery in the year 1954 that resistivity changes are induced in quartz-crucible-grown silicon by heat treatment to modest temperatures [64]. In subsequent research the centres were studied intensively by several experimental methods, among them electrical resistivity [65, 66], Hall effect [67, 68], infrared optical absorption [69, 70], photoluminescence [71, 72], deep-level transient spectroscopy [73, 74] and magnetic resonance [75, 76]. This has resulted in a vast amount of data on the properties of these intriguing defects, adding to their detailed understanding [77]. A first report on the observation of heat-treatment centres by magnetic resonance appeared in 1978 [40]. In this and following papers it was shown that by heat treatment in the thermal donor formation range two distinct paramagnetic centres are formed. Their EPR spectra were labelled Si-NL8 and Si-NL10.

Although distinctly different spectra belonging to centres with different structures, the two centres have much in common as demonstrated by the experimental observations. On the issue of similarity following facts can be listed.

- Both centres are formed by heat treatment in a temperature range typically from 400 to 500 °C in times varying from several hours to hundreds of hours. Though production kinetics are quite similar, NL8 tends to be formed in the earlier heat-treatment stages, whereas NL10 appears later [78]. The centres are lost by anneal above 500 °C.
- Both centres are observed in EPR as paramagnetic centres with a single unpaired electron spin $S = 1/2$. In the EPR spectra no hyperfine structure is discernible. The parameters of the spin Hamiltonian for spectrum NL10 are given in the Appendix.
- Although the spectra do not show a large anisotropy, their angular dependence could be measured to good accuracy in a K-band EPR spectrometer. Patterns corresponding to the orthorhombic-I symmetry were observed for both NL8 and NL10 [40, 79]. The centres thus possess a C_{2v} point-group symmetry implying a structure with a twofold symmetry axis and two perpendicular (011) mirror planes. In later papers a symmetry lowering towards monoclinic-I and triclinic has been reported [75, 80]. Nevertheless, the main symmetry character of the two centres remains close to orthorhombic. Corrections, which escape standard EPR resolution, are required in final defect modelling.
- Both spectra have g-tensor components close to, but somewhat smaller than the free-electron g value $g = 2.0023$. In an empirical classification both defects fall in the category of shallow donors, without broken bonds, and not involving any transition metal [81, 82].
- A rare feature of the g tensors of both NL8 and NL10 spectra is their dependence on the time of heat treatment [78, 79]. Upon extending the duration of the heat treatment the tensors gradually change towards more isotropic character. The effect for the NL10 defect is illustrated in Fig. 9, where the separation of the two resonances for the [111] direction of magnetic field is taken as a measure of anisotropy [80].
- The above-mentioned phenomenon of the g shifting is related to the existence of several species of the NL8 and NL10 groups. For the NL8 spectrum the family of species was directly observed in the optical absorption spectra of the related donor centres [69, 70]. The same species character applies for the NL10 defects. In EPR in the common X- and K-band frequencies the difference between g values of species is too small to be resolved. The development of discrete later species is observed as a continuous change of an average value. It has required the high resolution of high-frequency EPR to resolve individual species. Such experiments were reported recently [83]. A result comparing spectra recorded at the K-band frequency 23 GHz and at 349 GHz is given as Fig. 10.
- The required presence of oxygen for formation of NL8 and NL10 centres was commonly assumed from the earliest days because of production conditions, either requiring Czochralski silicon or silicon containing oxygen otherwise. This fact could be verified unambiguously by the observation of ENDOR of the ^{17}O isotope in the NL8 and NL10 spectra [84, 85]. From analysis of

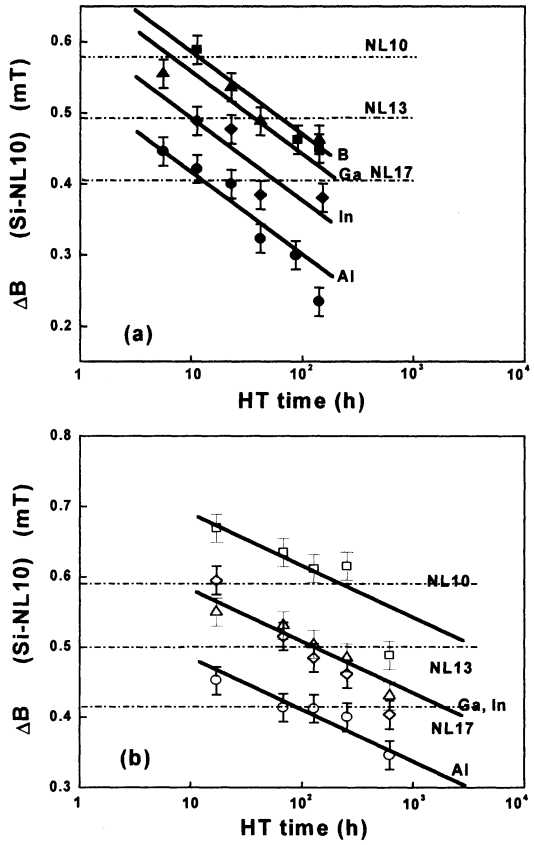

Fig. 9: Illustration of the g shift of EPR spectrum Si-NL10 observed in (a) crucible-grown and in (b) oxygen-diffused float-zoned p-type silicon with different acceptor doping. The magnetic-field difference between the two resonances for the [111] field direction is plotted as a function of the heat-treatment time at 470 °C. ΔB values as given for NL10, NL13 and NL17 are from Ref. 40.

the ENDOR data it was concluded that two oxygen atoms form the core of the heat-treatment centres [84]. They occupy the regular bond-centred sites, all in one (011) plane. The defect grows by addition of oxygen atoms, one by one, lowering the actual symmetry of some species to monoclinic-I.

- By measuring the ENDOR of the ^{29}Si isotope the wave function of the defect electron could be mapped for both NL8 and NL10. In an LCAO analysis of these results the localisations of the defect electron were determined to be small at many sites around the core [85, 86]. The wave functions have an extended character, even more for NL10 than for NL8; the result is typical for an electron bound in a shallow level.
- For both oxygen and silicon atoms on the (011) planes a considerable s-type density is found by

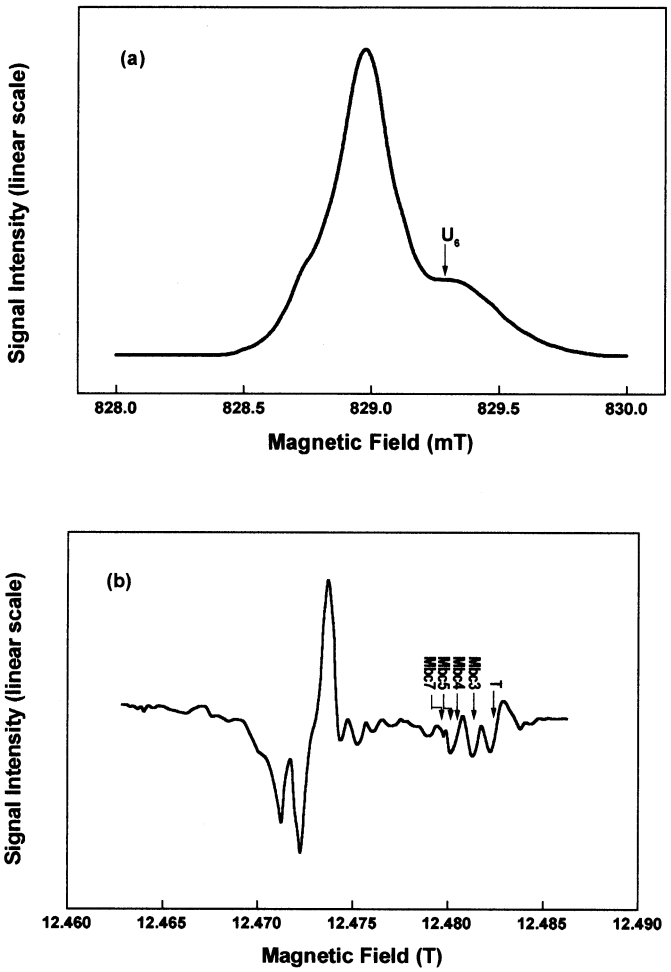

Fig. 10. EPR spectra Si-NL10 of a Cz-Si:Al sample after anneal at 470 °C for 200 h, observed (a) in K-band spectroscopy at 23 GHz and (b) at 349 GHz. Magnetic field ***B*** // [011]; resonances are labelled by U5, U1 and U6. For the high-frequency/high-field scan the resolved U6 components due to individual species are given the labels of their associated Al- ENDOR tensors.

the analysis. Without symmetry-forbidden planes the full A_1-type symmetry in orthorhombic approximation is deduced for the ground state [82].

In spite of these similarities the NL8 and NL10 defects are different. Whereas the NL8 spectrum could be assigned to the ionised state of the well-established thermal double donor [87], i.e., TDD^+, the identification of NL10 remains more difficult and puzzling. For the formation of the NL8 spectrum of the thermal double donor no impurities besides oxygen are required. In contrast, the NL10 spectrum does not uniquely belong to a single defect; rather, several defects with a different

structure do give NL10 resonances which are not distinguished in the EPR experiments. Such a complex situation has been clear from the outset when the role of aluminium doping was investigated. It was found that in the case of aluminium acceptor doping the formation of NL10 centres was enhanced considerably over that for other acceptors [78]. Consistent with this evidence aluminium ENDOR was observed on the NL10 spectrum [80, 88]. For the aluminium atom specific well-defined sites within the NL10 defect were concluded, for instance, an Al atom can take a position on the twofold defect axis. In an apparent contrast to this structure model, also NL10 spectra were observed in silicon certainly free of the required amount of aluminium doping or contamination. Hence, there must be alternative ways, maybe due to other impurities, of forming the structures yielding NL10 spectra. Specific investigations have shown that boron acceptors do not act like aluminium; ENDOR of the B impurity was absent in the NL10 spectra [89]. Oxygen-related donors, referred to as TD, ND and DD, are formed by heat treatment of n-type silicon; the slightly anisotropic g tensors of these defects as measured in the X band are in the NL10 range [90 – 92]. Extensive investigations were made on the formation of shallow donor centres by complexing of oxygen, nitrogen and carbon in silicon. These centres were observed in EPR with g tensors very similar or equal within error limits to the g tensor of NL10. On this basis it has been proposed that NL10 centres with C_{2v} symmetry actually arise from nitrogen-oxygen complexes, known as D(N,O) [93 – 95]. Attempts to observe an associated nitrogen hyperfine interaction on the spectra have so far been unsuccessful [95 – 97]. An isotropic spectrum, with $g = 1.999$, labelled NL10* and possibly identical to centres earlier labelled NL15 or NL18, is also reported to develop in these materials [95]. Recently, EPR signals were detected in hydrogenated Czochralski silicon after irradiation and thermal annealing corresponding to shallow donor centres named D1–D3. The principal values of the isotropic spectrum TU1 of donor D1 and of orthorhombic donor D2 are close to the NL10 values [98, 99]. In view of the participation of impurities in the NL10 defect hydrogen has to be considered as a prominent candidate. In the presence of hydrogen an accelerated formation of thermal donors was observed [100]. This was explained in theoretical studies as due to a considerable lowering of the activation energy for diffusion of oxygen through silicon when assisted by hydrogen [101]. As another manifestation of the hydrogen affinity to thermal donors their passivation by hydrogen has been observed [102], though the complexes were not stable up to the NL10 formation temperatures [74]. Confirming expectations hydrogen presence in the NL10 heat-treatment centre could be established by ENDOR measurements [75, 97]. Results illustrating two different methods to identify the impurity are given in Fig. 11. In the field shift method, Fig. 11(a), the ENDOR frequency is measured at a few values of the magnetic field. In the high-field approximation, expected to be valid in the present case, the shift is given by the spin Hamiltonian as $d\nu/dB = g_n\mu_N/h$, allowing the g_n value of the magnetic nucleus to be determined. For the measurement as illustrated one obtains $d\nu/dB = 42.6$ MHz/T, leading to $g_n = 5.59$. This result identifies the nucleus as hydrogen. In this field-shift method the nucleus producing the ENDOR effect can be identified on the basis of a single line. Fig. 11(b) illustrates the symmetric displacement of ENDOR transitions below and above the nuclear Zeeman frequency $\nu_Z = g_n\mu_N/h$.

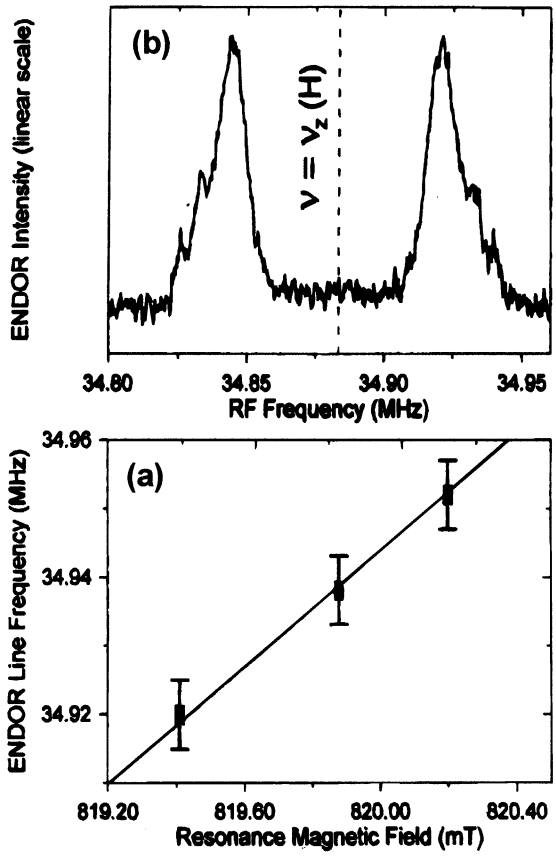

Fig. 11. ENDOR observed in Cz-Si:Al after 470 °C/55 h heat treatment. (a) Shift of an ENDOR frequency with magnetic field, with linear fitting function, (b) ENDOR lines close to the nuclear Zeeman frequency of hydrogen showing mirror-symmetry.

For the present case of measurements performed in a K-band spectrometer, the magnetic field of EPR observation is near 800 mT, with a nuclear frequency ν_Z around 35 MHz. The mirror-like symmetry of resonances with respect to ν_Z follows the spin-Hamiltonian solution $h\nu = h\nu_Z \pm (1/2)A_{eff}$, with A_{eff} the effective value of hyperfine interaction in the particular magnetic field direction.

In rotating the magnetic field from a [100] to a [011] direction in a (011) plane a complete angular dependence pattern as given by Fig. 12(a) is obtained [75, 103]. Following its analysis all spin-Hamiltonian parameters are determined. This again has unambiguously identified the hydrogen nucleus as the impurity involved in this NL10 ENDOR. The patterns displayed in Fig. 12(a) as preliminary fits to experimental data are based on hyperfine interaction tensors with the low triclinic

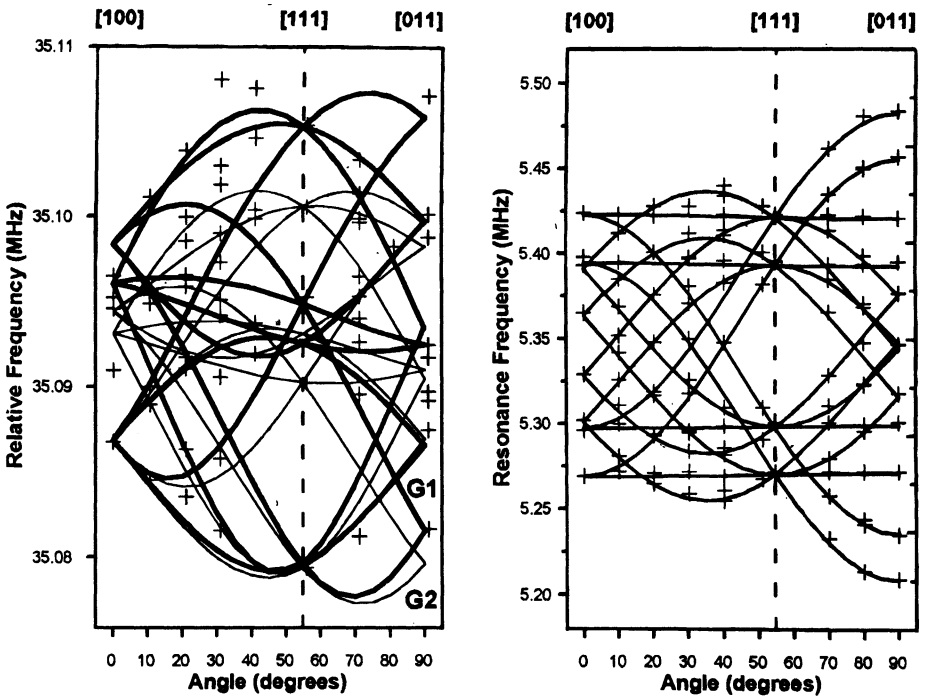

Fig. 12. Angular dependence patterns of Si-NL10 ENDOR. (a) Hydrogen ENDOR observed in Cz-Si:P sample after 470 °C/64 h heat treatment. Two triclinic hyperfine interaction tensors, G1 and G2, identified. (b) Deuterium ENDOR observed in Cz-Si:In sample after 470 °C/42 h heat treatment.

symmetry. They demonstrate a position of the hydrogen atom at a general site with respect to the defect core, not on one of its mirror planes, effectively reducing the defect symmetry to triclinic. There is only one hydrogen atom in each species. Analysing the hyperfine interaction in terms of an s orbital on the hydrogen atom, in the usual LCAO scheme, a low spin density is found on the hydrogen. As in other cases of hydrogen centres the bond is almost fully occupied by two electrons with opposite spin. For an NL10 spectrum observed in a deuterated sample one expects the hydrogen hyperfine frequencies to be scaled down by the ratio of the nuclear moments, i.e., by the factor $(g_n)_D/(g_n)_H = 0.15$. It is seen, however, in Fig. 12(b) that the observed ENDOR pattern has a much larger angular variation and, besides, shows a rather different symmetry [75, 104]. Actually for the deuteron, with its nuclear spin $I = 1$, the angular dependence is dominated by the quadrupole effect. To this interaction the unpaired spin electron makes only a minor contribution. The main effect comes from electrons in the hydrogen bond. The angular dependence as shown in Fig. 12(b) corresponds to an axial bond structure in a [011] direction perpendicular to the plane in which the oxygen atoms reside. The hydrogen atom sticks out of this mirror plane, in conformity with the

triclinic symmetry of the defect as a whole. With one hydrogen in its structure, the NL10 centre can be interpreted as the neutral charge state of a singly passivated thermal donor. The defect still has all the characteristics of a single donor. A detailed atomic model, putting all impurity atoms unambiguously on their proper place, is still lacking.

The above discussion exemplifies the power of magnetic resonance as a tool for determination of atomic and electronic structures of point-like defects in silicon. At the same time the thermal donor serves as an example to feel the limitation of the technique. In EPR none of the hyperfine interactions with the impurities, be it ^{17}O, ^{27}Al, ^{14}N, ^{1}H or ^{2}D, or with distant ^{29}Si was observed. From ENDOR it could be concluded that such interactions are small and not resolvable in EPR. Also, the species as separate components of both NL8 and NL10 defects are not resolved in the traditional measurement. X-band equipment, often used for thermal donor studies, is not particularly suitable. It has required the high-frequency EPR to observe some of this structure. Distinct NL10 defects, such as the NL10(Al) and NL10(H) structures, are not separated as well.

Quite likely, there exists a parallel between the existence of NL10 EPR centres with different atomic structures but electronically almost indistinguishable and the shallow thermal donors (STD's) observed in optical absorption, also produced by heat treatment. In the latter case slightly different absorption spectra are observed related to Al or H impurities in the samples [105, 106]. For the 1s to $2p_{\pm}$ transition of the STD(2) and STD(3) species an isotope effect correlated with hydrogen/deuterium substitution was observed, demonstrating a hydrogen involvement in these STD's [107]. A correlation between absorption strength in the infrared spectra and NL10 EPR intensities was reported, supporting the proposal of identifying optically observed STD centres with EPR centres in the NL10 category.

6. Hydrogen–chalcogen centres

As demonstrated by the occurrence of hydrogen–thermal-donor complexes, the interaction of hydrogen with double donors offers attractive opportunities for impurity-passivation studies. In contrast to passivated single dopants, one expects the complexes formed by partial passivation of dopants with double valency to be observable in magnetic resonance. This might be correlated with the binding of one or more hydrogen atoms to the impurity. Chalcogen impurities represent well-studied substitutional double donors in silicon [108]. Early passivation studies using the experimental method of deep-level transient spectroscopy showed that all chalcogen double donors, namely S, Se and Te, are passivated by binding hydrogen [11, 109]. Both band-gap levels were removed and no new levels were created. In contrast to this conclusion of full passivation, in infrared absorption five donor states were observed when hydrogen was diffused into sulphur-doped silicon [110]. Three of these spectra displayed a hydrogen/deuterium isotope effect.

Magnetic resonance experiments on the hydrogen-passivation of sulphur and selenium have been carried out as well [111, 112]. Following the bulk introduction of hydrogen by diffusion at

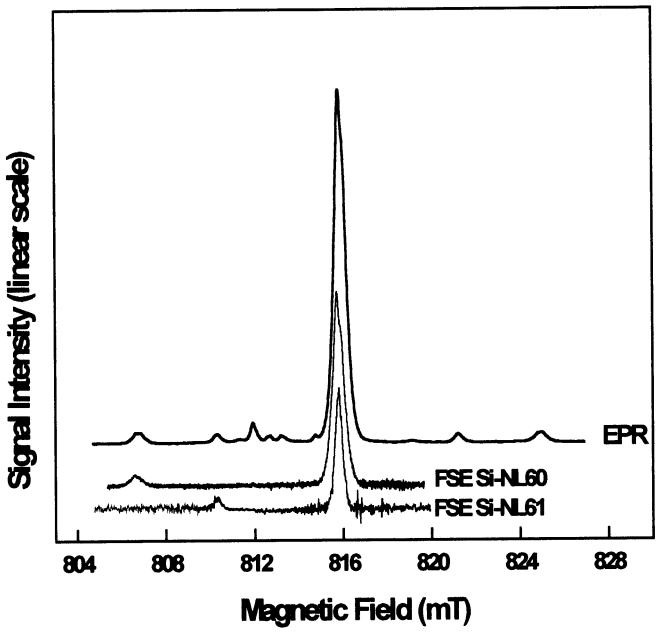

Fig. 13. Electron-paramagnetic-resonance (EPR) and field-scanned-ENDOR (FSE) scans of the Si-NL60 and Si-NL61 spectra of Se–H complexes over a range of magnetic field also covering the region of selenium hyperfine splitting; magnetic field $\boldsymbol{B}$ // [100]. Sample doped with natural selenium with 7.6% of the isotope ^{77}Se, nuclear spin $I = 1/2$.

high temperature the EPR spectra related to these chalcogen dopants and their pairs were replaced by new spectra, two in each case. For sulphur-doped material these were labelled Si-NL54 and Si-NL55; for the case of selenium doping the spectrum labels are Si-NL60 and Si-NL61. Fig. 13 illustrates the spectra NL60 and NL61 over the full range of magnetic field, whereas Fig. 14 shows the central part of the spectral region in higher resolution. Following the interpretation of the spectrum as due to Se–H complexes the strong central part, at around 816 mT in Fig. 13, corresponds to centres with the selenium isotopes with nuclear spin $I = 0$. The two pairs of satellites with offsets of about ±9.1 mT and ±5.4 mT, respectively, are due to the hyperfine interaction with the ^{77}Se isotope, having the nuclear spin $I = 1/2$. The relative intensity of these side lines is consistent with the 7.6% natural abundance of this isotope. The observed intensity indicates the presence of one selenium atom in the centre. To verify this conclusion spectra were also produced using selenium enriched to 99.1% in the ^{77}Se isotope. In the resulting spectra all intensity is found in the hyperfine components, the central line has vanished. In the experiments with sulphur, a very similar set of observations was made for the spectra NL54 and NL55. Sulphur-doped samples were

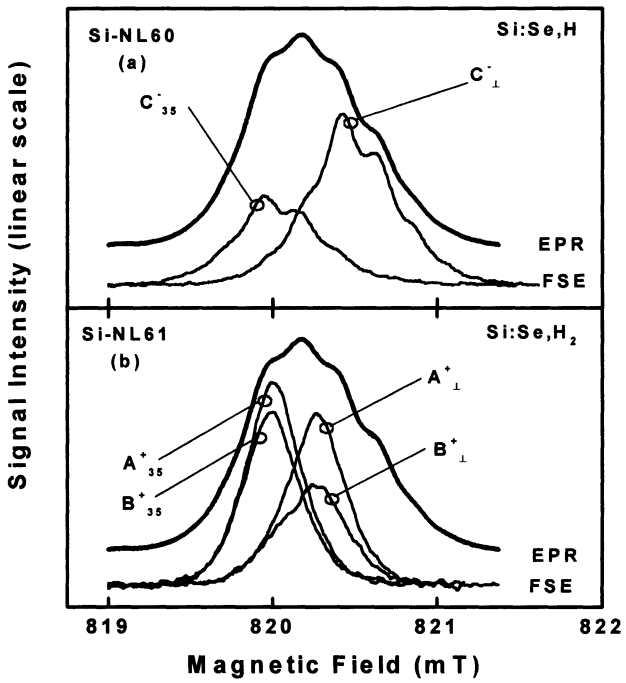

Fig. 14. Central part of the electron-paramagnetic-resonance (EPR) and field-scanned-ENDOR (FSE) spectra of Se–H complexes for magnetic field ***B*** // [011]. Labels $A^{+}_{\perp}$, etc., indicate the particular hydrogen-ENDOR transitions used for FSE selection (see Ref. 112). (a) FSE spectra of Si-NL60, (b) FSE spectra of Si-NL61.

prepared using natural sulphur, and also sulphur with an enrichment in the ^{33}S isotope of 25.5% and 99.5%. The ^{33}S nucleus has a spin $I = 3/2$, leading to a characteristic quartet hyperfine structure of four equal-intensity equidistant resonances. The ratio of intensities of the pairs of side lines is not constant, but depends on sample preparation conditions. For selenium it was found that a rapid thermal quench after diffusion favours the production of the outer pair of hyperfine lines, i.e., spectrum NL60, in the extreme case suppressing the formation of the NL61 spectrum completely. This provides one of the arguments to consider the spectra as belonging to different centres. For the sulphur spectra the effect of thermal treatment is much less pronounced. It may indicate a rather equal formation energy and thermal stability of the NL54 and NL55 centres. As regards the involvement of hydrogen in the centres, a structure due to hyperfine interaction with the nuclear moment of the proton, with $I = 1/2$, is just discernible in the side lines of the NL60 spectrum, Fig. 13. As in most of the centres discussed before, the hydrogen hyperfine interaction is small, and barely or not at all resolved in the standard EPR measurement. To observe and determine the hydrogen effect, the higher resolution of ENDOR is required. On all spectra extensive ENDOR measurements were made, using both the standard ^{1}H hydrogen and the ^{2}H deuterium isotopes with

100% enrichment. With all experiments carried out in a K-band spectrometer, with a microwave frequency of 23 GHz and consequently all EPR observed near the field B = 820 mT, the proton ENDOR is observed near the Larmor frequency 35 MHz and the deuteron spectrum near 5.3 MHz. From these ENDOR data the identification of hydrogen as part of the four EPR centres under discussion follows in an unambiguous manner. In the identification both the field-shift method and the recording of full angular-dependence patterns was applied. For the case of ^{2}H the nuclear spin $I > 1/2$ has allowed the nuclear quadrupole interaction to be measured. By the ENDOR a surprising distinction between sulphur and selenium passivation was revealed. On the EPR of spectrum NL61 two hydrogen ENDOR patterns with a small frequency difference were observed. Apparently, two distinct hydrogen atoms form part of this centre. All other spectra just have one hydrogen frequency.

With all spectral components resolved in ENDOR, the method of field-scanned ENDOR (FSE) utilising ENDOR tagging of spectral components, can be used for revealing underlying EPR. Results, as given in Fig. 13, assign the outer pair of selenium interactions to the NL60 spectrum, the inner pair to the NL61 spectrum. With FSE the structure in the central line which has multiple origins, is also resolvable, as shown in Fig. 14. As NL60 and NL61 have nearly equal g tensor, their resonances with $m_I = 0$, labelled C for NL60 and A and B for NL61, are nearly coincident in the central EPR line. Secondly, as the anisotropy is small, fine structure components for different orientations of the centres, labelled as perpendicular ($\perp$) or at an angle of 35 degrees (35) with the magnetic field, are also unresolved in standard EPR. Thirdly, the hydrogen hyperfine interaction of NL60 is resolved in its FSE spectrum. Under the improved conditions of FSE the angular dependence patterns of the individual components were recorded. In parallel to the foregoing qualitative description, the quantitative spectroscopic analysis of data was made with an appropriate spin Hamiltonian. All centres have electron spin $S = 1/2$, corresponding to a single unpaired spin. As all observed interactions give a <111> axial pattern, the tensors, i.e., Zeeman splittings g, hyperfine interactions A and quadrupole interactions Q, have the trigonal form. Parameters of the spectra are collected in the Appendix.

Following the experimental observations the hydrogen-passivated chalcogen centres are concluded to have a <111> axial structure. Assuming the S/Se atoms to stay on their regular substitutional site the hydrogen atoms must find a position on a <111> axis through this site. Three different types of sites may be distinguished: either between the chalcogen atom and a nearest-neighbour silicon atom on a bond-centred (BC) site, or further away from the chalcogen atom on the anti-bonding site of a nearest-neighbour silicon atom (AB-Si), or, finally, close to the chalcogen atom on an anti-bonding site (AB-S/Se). Which of such positions is actually taken by the hydrogen atom requires more subtle analysis of the hyperfine and quadrupole interaction parameters. Alternatively, the defect modelling is based on state-of-the-art theoretical calculations. An early treatment, predicting full passivation of the sulphur defect by one or two hydrogen atoms in forming complexes of monoclinic or orthorhombic symmetry, is at variance with presented experimental data [113]. In more recent research the interstitial BC and AB-Si sites were found to be stable

positions for hydrogen, with a small energy difference only [114]. In both cases a bond is formed with a nearest-neighbour silicon atom. This allows a plausible interpretation of experimental data by assigning the NL54 spectrum to the S–H complex with hydrogen on the BC site, with NL55 belonging to the complex with H on the AB-Si site. For selenium a similar agreement is obtained dealing with the more complex situation of binding one hydrogen atom in the NL60 and two in the NL61 centre [115]. Regarding their electronic structures, according to the g tensors the centres classify in the group of substitutional or interstitial donors with effective-mass-like ground states. By an LCAO analysis of hyperfine interactions with the nuclei ^{1}H or ^{2}D, ^{33}S or ^{77}Se, and ^{29}Si an informative mapping of the wave function can be obtained. As for other hydrogen-related centres and in agreement with the theoretical calculation [114] the spin density on the hydrogen is very low. On the chalcogen atoms the spin density η^2 is around 0.05, slightly less than the values of the isolated chalcogen impurities. Hyperfine interaction with ^{29}Si nuclei is too weak to give separated hyperfine lines; these interactions only contribute to the line width. The absence of strong hyperfine interactions is typical for the extended wave function of a relatively shallow donor. The neutral single-hydrogen centres may schematically be represented by a core (S/Se^{2+}–H^-) surrounded by electron e^- in an extended orbital. Summarising these analyses, the observed EPR centres are identified as one-chalcogen–one/two-hydrogen complexes with a trigonal atomic structure and with quite shallow donor character. Full passivation of the chalcogen double-donor activity did not take place by the hydrogen bonding.

7. Hydrogen–transition-metal centres

Transition metals are common fast diffusing impurities in silicon, easily present in the material as an unintentional contaminant, due to, e.g., insufficient control over purity in processing treatments. Nearly all of them introduce deep levels in the band gap of silicon, in this way having a profound effect on materials properties, in particular related to carrier recombination processes. Hydrogen atoms can be bound in the deep local potentials of the transition metal impurities and affect their properties substantially. Interaction between s states of hydrogen with d states of transition metals will lead to new defects with a possibly basically different electronic structure. It is certainly not obvious that hydrogen binding will lead to electrical passivation of these impurities. As a result of exchange coupling between spins in the d shells of transition elements states of high spin, compounded from orbital and intrinsic spin momenta, are formed (Hund's rule). It is not to be expected that the high spin will be nullified completely by binding one or more hydrogen atoms. Transition-metal–hydrogen complexes can still be paramagnetic, hence be observable by magnetic resonance, creating a field for fruitful studies of hydrogen-bonding physics.

The most detailed studies were performed on a centre identified as $[Pt_s(H_i)_2]^-$, which is observed in platinum-doped silicon after hydrogenation treatment typically for 24–72 hours at 1000–1250 °C [3, 116]. The spin resonance is described by electron spin S = 1/2 and shows the angular

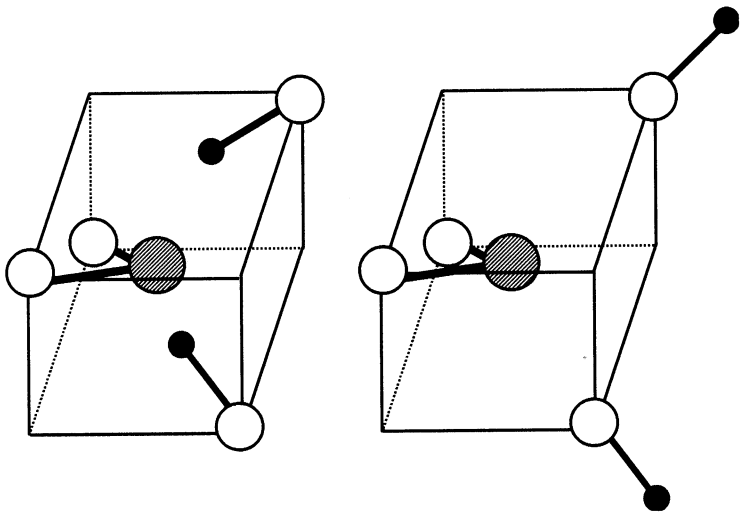

Fig. 15. Tentative models for the PtH_2 complex in silicon. Platinum atom shown shaded, hydrogen atoms shown as black spheres. (a) Hydrogen terminating bonds inwards into the vacancy, (b) H atoms pointing away from the platinum atom. Orthorhombic symmetry allows distortions of the centre which leave the (011) mirror plane symmetry. After Stavola, *et al.* [117].

dependence of an orthorhombic-I symmetry centre. The atomic structure is derived on the basis of the observed hyperfine interactions. The presence of one platinum atom is indicated by the resolved hyperfine splitting related to the ^{195}Pt isotope, nuclear spin $I = 1/2$ and natural abundance of 33%, resulting in the characteristic splitting of the resonance in three components with the intensity ratio of 0.25 : 1 : 0.25. Presence of two equivalent hydrogen atoms is revealed by triplet structure with amplitudes scaling as 1 : 2 : 1 of all resonances due to the hyperfine fields created by two hydrogen atoms (spin $I = 1/2$, 100%). In case of deuteration (spin $I = 1$) the associated hyperfine structure will have five components in the intensity ratio of 1 : 2 : 3 : 2 : 1, but their mutual separation will be reduced by the factor $2\mu_H/\mu_D \approx 6.5$. Due to the smallness of the splitting this has not been observed in resolved form, only as an appropriate line broadening. The spin-Hamiltonian parameters of the centre are given in the Appendix. A small difference of the g tensors and platinum hyperfine interaction was reported for the PtH_2 and PtD_2 centres [3].

Atomic models consistent with the observed symmetry and atomic constituents are given in Fig. 15 [117]. The model of the orthorhombic isolated Pt^- centre has provided an obvious starting point for modelling of PtH_2. Positions of the hydrogen atoms follow traditional chemical bonding arguments and are consistent with their hyperfine interactions with the defect electron. The isotropic part of hydrogen hyperfine interaction, $a = 8.6$ MHz [3, 4], corresponds to a localisation of around 0.6% on each of the two protons. The position of the hydrogen atoms on a nodal plane of the defect accounts in a natural manner for this small localisation. The still present non-vanishing component can be discussed in terms of many-electron effects, as in the case of centre Si-AA9. Anisotropic

hyperfine interaction with hydrogen nuclei must be due to electron spin localised on remote orbitals. From the reported values b = 0.6 MHz [3] or b = 1.1 MHz [4] and with equation (5) a distance R of 0.4 to 0.5 nm between electron and nucleus is calculated. Assuming one full electron spin to be present in the core position of the defect, the large distance found favours the hydrogen positions anti-bonding to silicon as sketched in figure 15(b). In experiment [3] hyperfine interactions with two ^{29}Si atoms have indicated a 26% localisation on these neighbours. In reality the wave function is therefore spread out over a larger region of the defect and the quantitative aspects of the model calculation should be taken with corresponding care.

A most important question is about the electrical activity of the PtH_2 centre. This has been probed by monitoring the effect of Fermi level on the observability of PtH_2 in its paramagnetic state. Fermi level changes were imposed by different platinum and/or donor doping concentration, by electron irradiation creating compensating acceptor centres and by illumination [4, 116]. As a result it was concluded that the paramagnetic state of the complex corresponds to $(PtH_2)^-$, and that a level $(PtH_2)^{2-}/(PtH_2)^-$ is positioned between E_{CB} – 0.045 eV and E_{CB} – 0.1 eV and another level $(PtH_2)^-/(PtH_2)^0$ between E_{CB} – 0.23 eV and E_{VB} + 0.32 eV. Hence, it must be concluded that hydrogenation of platinum-doped silicon leads to the formation of a double acceptor centre. Such conclusions are in remarkable agreement with results of other studies. From deep-level transient spectroscopy levels related to a PtH_2 defect were reported at E_{CB} –0.18 eV and E_{VB} + 0.40 eV [118 – 120]. Very recently published theoretical results place a first acceptor level at E_{CB} – 0.45 eV, but do not report a (2–/–) level [121]. In addition to the acceptor level the theoretical study finds a donor level close to the valence band, thus describing PtH_2 as an amphoteric defect. In the recent DLTS studies also electrical levels related to PtH_1 and PtH_3 are identified. The centre PtH_4 is considered to be a fully passivated Pt centre without electrical activity. In an early report on DLTS of hydrogenated platinum-doped n-type silicon the passivation of platinum was concluded [122]. Obviously in contradiction to the more recent observations, it may have occurred that the level at E_{CB} – 0.1 eV has been too shallow and the midgap level has been too deep for observation.

In a close parallel to the magnetic resonance the platinum–hydrogen complexes were investigated by optical absorption due to the local vibrational modes (LVM) of hydrogen [4]. Absorptions at 1888.2 cm^{-1} and 1901.6 cm^{-1} were identified as anti-symmetric and symmetric hydrogen stretching vibrations, respectively, in the paramagnetic state of PtH_2. Corresponding pairs of bands for the PtHD and PtD_2 centres are at the frequencies 1894.6 cm^{-1} and 1366.9 cm^{-1} for PtHD and at 1362.5 cm^{-1} and 1370.7 cm^{-1} for PtD_2. The isotope shifts confirm the presence of two hydrogen atoms in the centres. Vibrational spectroscopy is not restricted to the paramagnetic state of the complex. There are corresponding pairs of vibrations for the two other charge states. By varying the charge state of the defect, the changes in vibrational frequencies have helped to locate the levels. Probing the thermal stability of the PtH_2 centre it was found that the EPR spectrum anneals out by exposure to 500 °C for 3 hours [3] or to 600 °C [116]. The simultaneous loss of LVM spectra indicates that both spectra are associated with the same centre [116].

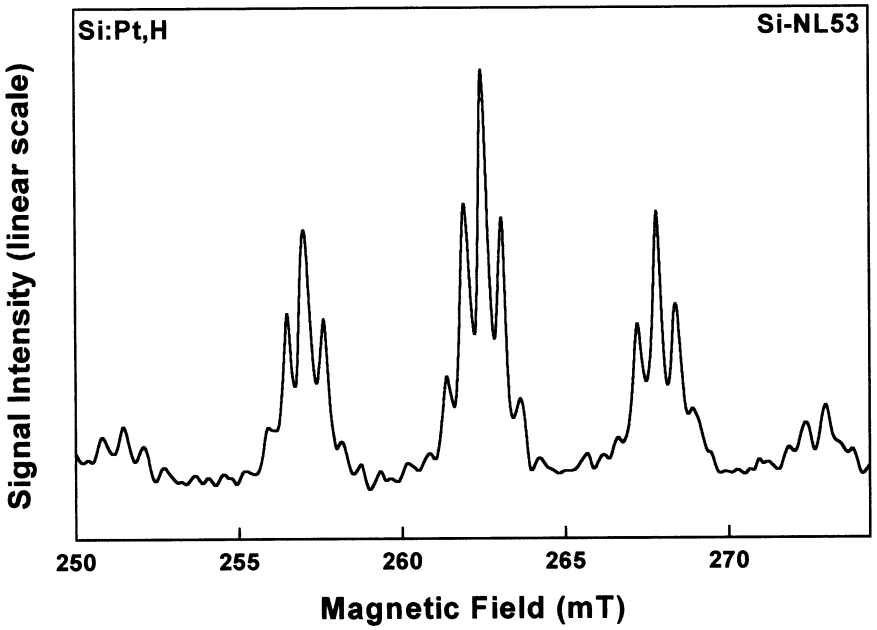

Fig. 16. Part of the Si-NL53 spectrum, recorded with the magnetic field parallel to a [111] crystal direction, at the microwave frequency of 9.2164 GHz and at temperature T = 7.5 K. Hyperfine structure due to three platinum atoms (isotope ^{195}Pt, I = 1/2, abundance 33%) and six hydrogen atoms (isotope ^{1}H, I = 1/2, abundance 100%) is exhibited. After Höhne, *et al.* [3].

Another spectrum of a more complex structure has been interpreted as arising from a trigonal $[Pt_s(H_i)_2]_3$ centre [3]. It is formed by hydrogenation of platinum-doped silicon when a retarded quenching procedure is applied. Centres revealing the tendency of platinum to coalesce into larger complexes with Si–Pt_3 groups as building blocks have earlier been identified [123, 124]. In the common way important atomic structure information is derived from the observed hyperfine interactions. For a centre with three equivalent platinum atoms a sevenfold line splitting should occur, each component corresponding to a distinct total m_I in the range –3/2 to + 3/2, in steps of 1/2. Given the abundance 0.33 of the magnetic isotope ^{195}Pt the expected intensities must reflect the ratios 0.01 : 0.13 : 0.57 : 1 : 0.57 : 0.13 : 0.01. As shown in Fig. 16 such a structure is actually observed, with the reservation, however, that the two outermost lines are missing; due to their weakness they are below the noise level. As also shown in Fig. 16, each of the ^{195}Pt components has characteristic identical further structure, which is caused by hydrogen hyperfine effects. As the number of components in this latter structure is odd, there must be an even number of hydrogen nuclei responsible for it. From comparison with the observed spectra this number of hydrogen atoms is deduced to be six. Predicted intensities scaling as 1 : 6 : 15 : 20 : 15 : 6 : 1 are in good

agreement with experimental line heights. Besides, six hydrogen atoms can easily be incorporated in a defect model of the required trigonal symmetry. Spin-Hamiltonian parameters of the spectrum, known under label Si-NL53, are given in the Appendix. As for PtH_2 also for the present centre the electron spin localisation on the hydrogen is small, again near 0.6%. It should be noted that in the defect model as presented in Ref. [3] the hydrogen atoms are not finding their positions on a symmetry plane with a node of electron density. To explain the low spin density the effective pairing-off of spins in the hydrogen bond has to be invoked, as for several others of the hydrogen-related centres. As was found for the PtH_2 defect, also the NL53 centre is observed as a so-called bulk defect in silicon samples with minimum dimensions of more than 1 mm. Mechanically removing a layer of about 10 μm thickness all over the sample surface did not notably reduce the signal intensity. It follows that centres throughout the volume of the samples become hydrogen bonded using the introduction method of high-temperature diffusion. It is this bulk passivation that has allowed the powerful but less sensitive tools of optical and magnetic resonance spectroscopy to be employed for defect characterisation. This forms an apparent contrast with other common introduction techniques as chemical etching, ion implantation and plasma treatment.

Recently, hydrogenation of silicon doped with gold, the other late 5d element that acts an effective deep-level carrier recombination centre, was investigated with magnetic resonance. At least one gold–hydrogen complex was observed [125 – 127]. Parameters of the associated spectrum labelled Si-NL64 are included in the Appendix. The centre has the more rare triclinic symmetry. For some field orientations spectral lines show a well-resolved structure into 12 components in the ratios of (1 : 2 : 1) : (1 : 2 : 1) : (1 : 2 : 1) : (1 : 2 : 1). Fig. 17 gives an illustration. It is hard to escape the conclusion that the centre contains one gold atom (^{197}Au, I = 3/2, abundance 100%) and two hydrogen atoms. In the triclinic overall structure two hydrogen atoms cannot be strictly on equivalent sites in the defect. From the 1 : 2 : 1 hydrogen-related structure one concludes that the hydrogen atoms find themselves on sites with a near-identical local structure. As a result, lines are coinciding within experimental resolution. Given the triclinic symmetry of the AuH_2 centre one cannot view the centre as an exact counterpart of the orthorhombic PtH_2 centre. Nevertheless, upon closer inspection and analysis, strong similarities come to light. Considering first the hyperfine interaction with the transition element it appears that their principal values, as given in the Appendix, are very nearly proportional to the respective nuclear g values of the gold and platinum isotopes (^{195}Pt: g_n = 1.2190, ^{197}Au: g_n = 0.09717), implying equal spin localisation in this core part of the centres. The same conclusion holds for the hydrogen hyperfine interactions. In both cases the isotropic part a is near 9 MHz and the anisotropic part b near 1 MHz, resulting in the same conclusions for AuH_2 on localisation 0.6% and distances as discussed for PtH_2. In the region of the impurities the two defects therefore show a strong resemblance allowing to use the well-established PtH_2 model as a starting point for AuH_2. Neutral gold is iso-electronic to negative platinum. Quite likely spectrum Si-NL64 corresponds to the $[Au_s(H_i)_2]^0$ centre observed in the neutral paramagnetic state. For yet unknown reasons the gold–hydrogen centre has distorted to lower symmetry. The EPR centre might well be identical to the AuH_2 centre reported in DLTS studies [128 – 130]. This

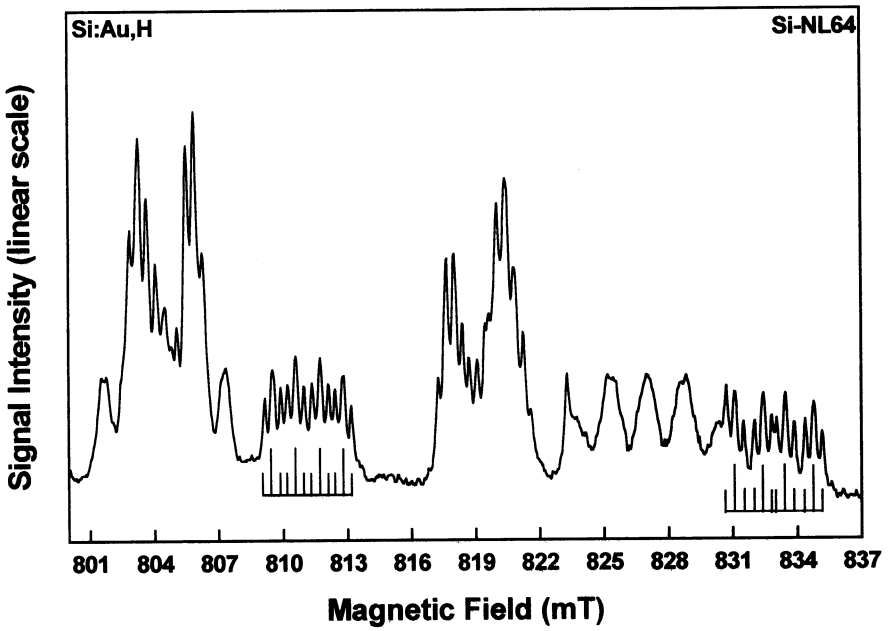

Fig. 17. Part of the Si-NL64 spectrum, recorded with the magnetic field in the (0,–1,1) plane about 10° away from [011], at the microwave frequency of 23.0217 GHz and at temperature T = 4.2 K. Hyperfine structure due to one gold atom (isotope ^{197}Au, I = 3/2, abundance 100%) and two hydrogen atoms (isotope ^{1}H, I = 1/2, abundance 100%) is exhibited. After Huy and Ammerlaan [125].

passive complex, escaping direct detection, is proposed to exist on the basis of annealing kinetics in the gold–hydrogen system. Another centre, AuH_1, electrically active with three band-gap levels, has found no counterpart yet in magnetic resonance [129, 131]. The complexes containing Au and H have vibrational properties similar to the PtH and PtH_2 complexes [132, 133].

Further understanding of the microscopic structure of the complexes, which involved transition metal and three hydrogen atoms has, very recently, been achieved following the observation of a one-platinum–three-hydrogen (PtH_3) centre by electron paramagnetic resonance [125 – 127]. In Fig. 18 a typical EPR spectrum of the PtH_3 centre, labelled Si-NL65, observed in platinum-doped wet-hydrogenated silicon, is depicted for the magnetic field parallel to the <011> crystallographic direction of the sample, at temperature T = 4.2 K, microwave frequency f = 22.71368 GHz, and under visible-light illumination. The spectrum is characterised by a resolved hyperfine structure of 1:3:3:1 – 4:12:12:4 – 1:3:3:1 obviously revealing the presence of one platinum atom (I = 1/2, 33.8% natural abundance) and three equivalent hydrogen atoms (I = 1/2, 100% natural abundance). Also,

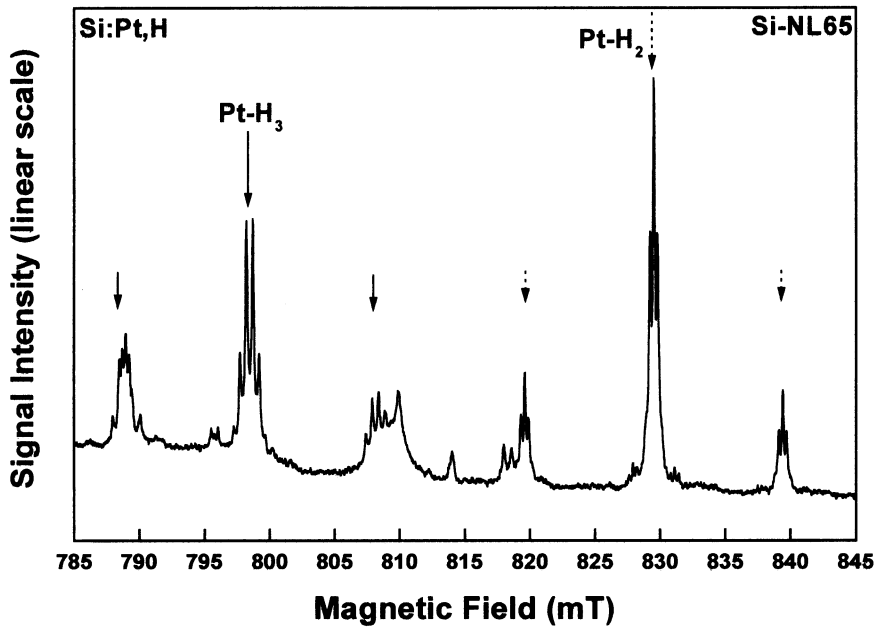

Fig. 18. Part of EPR spectrum of the Si-NL65 centre observed in the platinum-doped hydrogenated silicon samples for magnetic field parallel to <011> crystallographic direction, temperature T = 4.2K, microwave frequency f = 22.71368 GHz. The spectrum is observed under visible-light illumination revealing hyperfine structure of 1:3:3:1 – 4:12:12:4 – 1:3:3:1 as due to the hyperfine interaction with one platinum and three equivalent hydrogen atoms. The spectrum of the well-known PtH_2 is also observed and indicated. Due to superposition with some other centre, the low-field hyperfine lines of the Si-NL65 spectrum are unresolved.

the spectrum of the well-known PtH_2 centre is observed and indicated. As previously predicted from theoretical works, a defect of one-platinum and three-hydrogen atoms should have trigonal symmetry [121, 134]. Indeed, the symmetry of the Si-NL65 spectrum is trigonal with a large anisotropic hyperfine interaction of platinum and a slight anisotropy of the hydrogen hyperfine interaction. Details of the spin-Hamiltonian parameters of the spectrum are given in the Appendix. Analysis of the experimentally observed data of the PtH_3 centre using the standard LCAO treatment have disclosed surprisingly similar values of the hydrogen hyperfine interaction as compared to that of the PtH_2, AuH_2, as well as the $[PtH_2]_3$ centres. With the anisotropic part b = 0.9 MHz and isotropic part a = 13.67 MHz, these values, again, imply a localisation of about 0.95% on each of the three protons and a distance of about 0.5 nm between electron and nucleus. From these results, microscopic models for the PtH_3 centre have been proposed in which the platinum atom occupies a substitutional site, three hydrogen atoms are interstitial anti-bonding to three silicon nearest-

neighbour atoms and arranged themselves with trigonal symmetry about a <111> trigonal axis. Taken into account the fact that the $[PtH_2]^-$ centre is paramagnetic in the negative charge state, the Si-NL65 spectrum of the PtH_3 centre most probably is observed in the neutral paramagnetic charge state, i.e., $[Pt_s(H_i)_3]^0$. It should be noted that the formation of the PtH_3 centre is in strong competition with the formation of the neutral interstitial iron centre $(Fe_i)^0$, the PtFe pair as well as the other Pt-Pt pairs, resulting in a very low formation probability of the centre. This explains the absence of detection of this centre by magnetic resonance in the past.

Deep-level transient spectroscopy has made substantial contributions to the understanding of reactions between hydrogen and transition elements [135]. Besides gold and platinum, the hydrogen interaction processes were studied for the 4d elements rhodium [136], palladium [119, 137, 138] and silver [10, 119, 131] and for the 3d elements titanium [119, 139], vanadium [140, 141], chromium [141], cobalt [119, 142, 143], nickel [119, 144] and copper [145]. Reports on magnetic resonance characterisation are scarce. Besides platinum and gold, they are limited to iron [146] and palladium [126, 127], suggesting a fruitful field of future research left uncovered.

8. Other hydrogen-related centres

By thermal treatment new hydrogen-related centres can be formed through redistribution of hydrogen becoming available by thermally-activated dissociation with subsequent trapping into sites which provide more stable bonding. Fig. 6 illustrates an annealing sequence in which several centres, including AA1 [19], AA2 [47], AA3 [19], AA10 [18] and AA11 [19], are involved. By such a process of thermal anneal recently the trigonal centre AA17 was created in high-purity silicon (resistivity 3000 Ohm.cm) [147]. The centre anneals in at 200 °C; it anneals out at 450 °C. Prior to the thermal treatment, hydrogen was uniformly introduced, either by 30 MeV proton implantation or by high-temperature diffusion in a wet atmosphere. Without involvement of other impurities than hydrogen, the tentative model for the centre is based on an intrinsic silicon defect. The core of the AA17 defect is proposed to consist of a {111} planar hexa-vacancy. The hexa-vacancy as a very stable fundamental intrinsic defect in silicon has been described theoretically but has escaped detection as the defect has no band-gap level [148]. Two hydrogen atoms find their equivalent positions on the [111] axis through the centre of the six-fold ring, one on each side of the plane. In order to account for the zero-field splitting D by dipole–dipole coupling the distance between the hydrogen atoms must be around 1.2 nm, equal to 5 silicon–silicon nearest-neighbour distances. The spin localisation on the hydrogen atoms is 31%, with 9% s and 91% p character, typical for a vacancy like defect. The defect is observed in its neutral state with an even total electron number. The two electrons on the hydrogen sites couple to an electron spin $S = 1$. Hydrogen hyperfine structure was not noticeable in the AA17 spectra. The conclusion about hydrogen participation in the centre is based on the strong dependence of the formation rate on hydrogen content. Conditions of formation and temperature range of stability of the AA17 EPR

centre and the luminescent centre B_{41} (1.1509 eV) of an optically active hydrogen dimer are very similar [149 – 151]. It is suggested on that basis that both spectra derive from the same defect. The centre is considered to be a precursor for hydrogen platelet formation. Spin-Hamiltonian parameters of the AA17 centre are tabulated in the Appendix.

By being present as a mobile reactive agent, hydrogen can have its role in the anneal of radiation effects. In such studies, it has been observed that in silicon subjected to bombardment with H^+ ions the thermal annealing of radiation defects occurred at a lower temperature and gave a more full recovery of the electrical conductivity [152]. Also the annealing of so-called vacancy-void centres was accelerated by proton irradiation [153].

A remarkable property of hydrogen is its ability to enhance the mobility of other impurities in silicon. The phenomenon has been observed for oxygen, the most common impurity in silicon, and, more recently, for aluminium. Oxygen represents the best documented case investigated experimentally and theoretically [154]. In their equilibrium state, oxygen atoms occupy bond-centred sites midway between two silicon atoms and diffuse by jumping over these positions in a process requiring 2.56 eV of activation energy [155]. In the presence of nearby hydrogen the Si–O–Si bond is strongly weakened by the formation of a hydrogen bond. Static and dynamic theoretical models express different views on whether an H–Si [101, 156] or an H–O [157] configuration characterises the intermediate diffusion state, but agree that the barrier for oxygen motion is reduced by a factor of almost two. In these diffusion mechanisms hydrogen plays a catalytic role; it participates in the process without being consumed. In the experiments, the effect of hydrogen enhancement of oxygen mobility is observed in the temperature range around 300 °C. Both single jump processes such as the recovery from stress-induced dichroism as well as long-range oxygen migration in oxygen loss processes with correlated thermal donor formation are accelerated in the presence of hydrogen atoms, e.g., from a plasma source [158 – 160]. Under conditions, hydrogen can become a component of an oxygen cluster, as it happens in the NL10 thermal donor. In case of aluminium, the conclusion of enhanced impurity diffusion rests entirely on the observation of the Si-AA15 spectrum [161]. To form the centre silicon samples were hydrogenated and irradiated at low temperature, around 80 K. Upon anneal at 180 K the two centres AA15 and AA16 emerge [162 – 164]. Centre AA16 is a one-aluminium centre and corresponds to a rapidly diffusing species, presumably an Al_i–H complex. Centre AA16 is no longer observable after anneal at 200–220 K. Centre AA15 remaining until anneal at 300 K is identified as an Al_i–Al_i interstitial pair. From its hyperfine structure with 11 groups of lines it is unambiguously concluded that the centre has two aluminium atoms as its components. It has required long-range migration over distances of around 100 lattice sites to bring these two atoms together. Under the conditions of the experiment, without any carrier injection or generation, a process of recombination enhanced a-thermal diffusion is sufficiently suppressed. In the model, the two aluminium atoms in the AA15 centre are on equivalent sites in an undistorted lattice, but an additional distortion lowers the symmetry to monoclinic-I and renders the two Al sites slightly different. The distortion is most easily explained by a nearby additional impurity, for which the only candidate is hydrogen. If so, the hydrogen

actively participates in the final defect structure and its role is more than just a catalyst. It must be noted that neither for AA15 nor AA16 the presence of hydrogen in the defect structure is supported by discernible hyperfine interaction with the impurity. Above examples illustrate the role the hydrogen impurity fulfils in stimulating fundamental diffusion studies in the covalent silicon host on a microscopic level. The relevance of enhanced migration rates of oxygen and aluminium, by orders of magnitude under circumstances, for the materials science of silicon is obvious. Being conscious that hydrogen can be present as an unknown unintentional impurity in silicon, as a result of some processing treatment, the control over hydrogen and its physics in silicon has become an important topic.

A special category of paramagnetic centres of silicon is formed by surface- and interface-related defects. If a silicon crystal is terminated by, for instance, a flat (111) surface, a density of 7.8×10^{14} cm^{-2} of surface atoms present a dangling bond in a [111] direction into free space. In order to passivate these electrically active states in standard device practice a thermal oxide is grown on the surface. However, due to lattice mismatch and to relieve strain in the interface a typical number of 0.5 to 1.5% of surface states is not terminated by the oxide [165, 166]. These centres are paramagnetic in their neutral state and give a magnetic resonance spectrum known as the P_b centre [167, 168]. Often the centre is represented by the symbol $-Si{\equiv}Si_3$ indicating the one dangling bond and the three fully occupied bonds to silicon atoms in the first sub-surface layer. Following this microscopic model the centres have a trigonal symmetry, in agreement with EPR characteristics, as given in the Appendix [169, 170]. Already in the first paper on the P_b centre it was noted that hydrogen can bleach the P_b resonance [167]. In more systematic studies it was found that hydrogen can both passivate and depassivate the P_b centres [165, 171]. In a temperature region from 220–260 °C a reaction $P_b + H_2 \rightarrow HP_b + H$ leads to full passivation of the interface centres forming HP_b or $H{-}Si{\equiv}Si_3$. These diamagnetic HP_b centres are unobservable in EPR. At higher temperature, in the range 500–590 °C, the P_b centres are recreated by a reaction $HP_b \rightarrow P_b + H$. For the technologically more important (100) Si/SiO_2 interface the situation is more complex as two interface centres, P_{b0} and P_{b1}, exist. The dominant defect at the (100) interface, P_{b0}, is not chemically equivalent to the (111) P_b centre in spite of similar g tensors [172]. It was found that the hydrogen passivation is described by similar reactions as mentioned above for all types of interface defects, P_b, P_{b0} and P_{b1} [173]. In addition to it role as passivation agent of P_b, hydrogen takes part in the centre as a chemical constituent not affecting its paramagnetic state. By ENDOR hyperfine interactions with hydrogen close to the Larmor frequency have been detected [174, 175]. A number of specific sites for the hydrogen atoms could be indicated. These hydrogen atoms appear to have a minor effect only on the global defect properties. Variations related with these atoms as a P_b decoration may well be responsible for minor variations in the P_b parameters from different sources in the literature or from P_b centres grown in different interface structures [169, 170, 176]. A very similar spectrum has been reported under the label Si-NL52 [177]. As the spin-Hamiltonian data in the Appendix show, the g tensor of this trigonal centre has similar, though not identical, values as P_b. These principal values are characteristic for an electron in a (111)-oriented sp^3 hybrid orbital. Several other centres

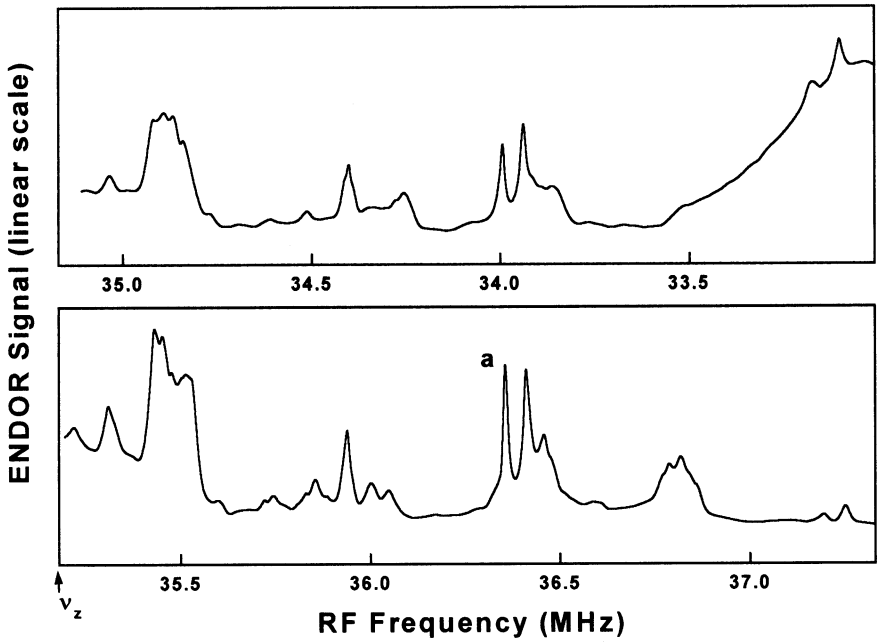

Fig. 19. ENDOR scan on the Si-NL52 EPR spectrum, magnetic field B = 826 mT, in (011) plane, 5° away from the [011] direction. The scan is cut at the nuclear Zeeman frequency of hydrogen, ν_Z = 35.168 MHz for field B. The low-frequency part of the scan is folded back to more clearly show the symmetric pattern with respect to ν_Z, as required for hydrogen ENDOR.

with a well-established structure provide a basis for an empirical relation between g tensor and electronic structure. In this category of defects one finds the phosphorus–vacancy complex (spectrum G8, $g_{//}$ = 2.0005, $g_{\perp}$ = 2.0104, Ref. 23), the negative di-vacancy (spectrum G7, $g_{//}$ = 2.0012, $g_{\perp}$ = 2.0142, Ref. 178), the penta-vacancy (spectrum P1, $g_{//}$ = 2.0020, $g_{\perp}$ = 2.0111, Ref. 179) and the B centre (spectrum G16, $g_{//}$ = 2.0026, $g_{\perp}$ = 2.0096, Ref. 180). Even more compelling evidence for the (near-) identical structure of the two centres follows from the equal hyperfine interaction with the silicon atom on which the dangling bond resides. Standard LCAO analysis of these hyperfine parameters yield an electron localisation η^2 = 0.66, with 11% s and 89% p character, for both defects.

On this basis one is tempted to conclude to identity of the P_b and NL52 centres. However, some differences, hard to ignore, are also revealed by the experiments. Centre NL52 is produced by hydrogen implantation as a bulk defect, in high-resistivity float-zoned silicon without appreciable amount of oxygen present. Spectrum NL52 is therefore produced under conditions not providing some of the basic requirements as established for P_b. Also in the spectral characteristics of NL52 some features are observed which are absent for P_b. In the EPR of NL52, for $\boldsymbol{B}$ // [111] the line

shape of the single orientation with axis parallel to the field, the resonance line has a four-component structure which is interpreted as hyperfine structure due to two inequivalent hydrogen atoms. Such structure was never reported for the P_b centre. Identification of the structure is supported by ENDOR on this resonance revealing spectra as shown in Fig. 19 [181]. From the symmetry of the ENDOR spectrum with respect to the hydrogen Larmor frequency, and independently by applying the field-shift method, resonances were unambiguously identified as hydrogen interaction. Actually, the ENDOR spectrum of Fig. 19 revealing a multitude of hydrogen-related resonances represents the first hydrogen ENDOR reported for a point defect in silicon. A full analysis of the angular dependence of ENDOR frequencies is not yet available. Positions of the hydrogen atoms within the NL52 structure are therefore not known. Hydrogen ENDOR frequencies observed for NL52, in the range 1–10 MHz [181], are substantially larger than those reported for P_b, which are in the range 100–400 kHz [175]. A best identification of the NL52 centre is that of a P_b-like defect with hydrogen atoms included on specific defect sites. Hydrogen interactions with P_b and P_b-like centres include decoration and passivation. Further investigations are required to unravel the details of probably a rich set of interactions.

Acknowledgements

The authors are grateful to R. J. Dirksen, Yu. V. Gorelkinskii, T. Gregorkiewicz, M. Höhne, U. Juda, Yu. V. Martynov, R. C. Newman, P. Stallinga, L. S. Vlasenko and I. S. Zevenbergen for contributions of various kinds resulting from joint research on hydrogen in silicon by magnetic resonance.

Appendix. Parameters of magnetic resonance spectra related to hydrogen in crystalline silicon.

Spectrum/model: Si-AA9/$(H_{BC})^0$

Symmetry: trigonal, point group $\bar{3}$m, symmetry type a_{1u}

Electron spin: $S = 1/2$

g Tensor: $g_{//[1,1,1]} = 2.0011$, $g_{\perp[1,1,1]} = 1.9983$

A Tensor: nucleus ^{1}H, spin $I = 1/2$, abundance 100%, mass $m_p = 1837.15m_e$, $g_p = 5.5856$, 1 site
$A_{//[1,1,1]} = -6.2$ MHz, $A_{\perp[1,1,1]} = -31.4$ MHz, $a = -23.0$ MHz, $b = 8.4$ MHz

A Tensor: nucleus ^{29}Si, spin $I = 1/2$, abundance 4.7%, $g_{Si} = -1.11052$, 2 sites
$A_{//[1,1,1]} = -139.0$ MHz, $A_{\perp[1,1,1]} = -72.9$ MHz, $a = -94.9$ MHz, $b = -22.0$ MHz

Model: neutral hydrogen atom on bond-centred site (BC) between silicon atoms, anneals out at 200 K

References: 7, 18, 19, 26, 29, 182 – 185

Spectrum/model: Si-Mu*/muonium

Symmetry: trigonal

Electron spin: $S = 1/2$

g Tensor: $g \approx 2$

A Tensor: positive muon μ^+, spin $I = 1/2$, mass $m_\mu = 207.769m_e$, $g_\mu = 2.0016$, 1 site
$A_{//[1,1,1]} = -16.82$ MHz, $A_{\perp[1,1,1]} = -92.59$ MHz, $a = -67.33$ MHz, $b = 25.26$ MHz

A Tensor: nucleus ^{29}Si, spin $I = 1/2$, abundance 4.7%, $g_{Si} = -1.11052$, 2 sites
$A_{//[1,1,1]} = -137.5$ MHz, $A_{\perp[1,1,1]} = -73.96$ MHz, $a = -95.14$ MHz, $b = -21.18$ MHz

Model: muonium atom on bond-centred site (BC) between silicon atoms

References: 7, 19, 20, 22, 182 – 184, 186

Spectrum/model: Si-HSD

Symmetry: cubic

Electron spin: $S = 1/2$

g Tensor: $g = 1.99875$

Model: electron in conduction band, resulting from ionisation of the hydrogen-associated shallow donor (HSD)

References: 7, 34

Spectrum/model: Si-AA1/HDD^+

Symmetry: orthorhombic-I

Electron spin: $S = 1/2$

g Tensor: $g_{//[1,0,0]} = 1.9997$, $g_{//[0,1,1]} = 1.9947$, $g_{//[0,-1,1]} = 2.0009$

Model: hydrogen-related double donor in positive charge state, anneals in at 350 °C, anneals out at 550 °C

References: 7, 19, 37, 42, 187

Spectrum/model: Si-NL51

Symmetry: tetragonal

Electron spin: $S = 1$

g Tensor: $g_{//[1,0,0]} = 2.00707$, $g_{\perp[1,0,0]} = 2.00069$

D Tensor: $D_{//[1,0,0]} = -37.9$ MHz, $D_{\perp[1,0,0]} = 19.0$ MHz

Model: possibly similar to B3 centre

References: 7, 44

Spectrum/model: Si-AA2

Symmetry: triclinic

Electron spin: $S = 1/2$

g Tensor: $g_1 = 2.0020$, // (+0.2917, +0.7814, +0.5517)

$g_2 = 2.0073$, // (+0.7764, –0.5303, +0.3406)

$g_3 = 2.0074$, // (–0.5587, –0.3290, +0.7613)

A Tensor: nucleus ^{29}Si, spin $I = 1/2$, abundance 4.7%, $g_{si} = -1.11052$

$A_{//} = (-)358$ MHz, // (+0.532, +0.691, +0.490)

$A_{\perp} = (-)225$ MHz, $\perp$ (+0.532, +0.691, +0.490)

Model: hydrogen implantation, anneals in at 600 °C, anneals out at 700 °C, vacancy cluster with trapped hydrogen

References: 19, 37, 47

Spectrum/model: Si-AA3

Symmetry: triclinic

Electron spin: $S = 1/2$

g Tensor: $g_1 = 2.0014$, // (+0.2988, +0.1658, +0.9398)

$g_2 = 2.0029$, // (+0.4742, –0.8804, +0.0046)

$g_3 = 2.0040$, // (+0.8282, +0.4443, –0.3417)

Model: hydrogen implantation, anneals in at 350 °C, anneals out at 550 °C

References: 19, 48

Spectrum/model: Si-AA10

Symmetry: monoclinic-I

Electron spin: $S = 1/2$

g Tensor: $g_{//[0,1,1]} = 2.0021$, $g_{\perp[0,1,1]} = 1.9943$, $g_{\perp[0,1,1]} = 2.0011$, $\theta = 16.6°$

Model: hydrogen implantation in Czochralski silicon, anneals out at 200 K

References: 18, 19

Spectrum/model: Si-AA11

Symmetry: monoclinic-I

Electron spin: $S = 1/2$

g Tensor: $g_{//[0,1,1]} = 2.0125$, $g_{\perp[0,1,1]} = 2.0035$, $g_{\perp[0,1,1]} = 2.0115$, $\theta = 37.0^{\circ}$

Model: anneals out at 270 °C

References: 19

Spectrum/model: Si-S1

Symmetry: trigonal

Electron spin: $S = 1/2$

g Tensor: $g_{//[1,1,1]} = 2.0010$, $g_{\perp[1,1,1]} = 2.0103$

Model: superposition of centres $(VH)^0$, $S1_a$ and $S1_b$, hydrogen ion implantation, anneals out at 300 °C

References: 5, 6, 7, 19, 49 – 52, 54, 188 – 190

Spectrum/model: Si-$(VH)^0$

Below 65 K

Symmetry: monoclinic-I

Electron spin: $S = 1/2$

g Tensor: $g_{1,\perp[0,1,1]} = 2.0090$, $g_{2,//[0,1,1]} = 2.0114$, $g_{3,\perp[0,1,1]} = 2.0006$, θ(axis 3, [0,1,-1]) = 32.4°

A Tensor: nucleus ^1H, spin $I = 1/2$, abundance 100%, 1 site

$A_1 = -3.3$ MHz, $A_{2,//[0,1,1]} = -4.6$ MHz, $A_3 = 8.5$ MHz, $\theta = 8.0^{\circ}$

A Tensor: nucleus ^{29}Si, spin $I = 1/2$, abundance 4.7%, 1 site, trigonal within error limits

$A_1 = -275$ MHz, $A_2 = -275$ MHz, $A_{3,//[1,1,1]} = -435$ MHz, $\theta = 35.3^{\circ}$

A Tensor: nucleus ^{29}Si, spin $I = 1/2$, abundance 4.7%, 2 equivalent sites

$A_1 = -27$ MHz, $A_2 = -27$ MHz, $A_{3,//[1,1,1]} = -34$ MHz, $\theta = 35.3^{\circ}$

A Tensor: nucleus ^{29}Si, spin $I = 1/2$, abundance 4.7%, 3 equivalent sites

$A_1 = -25$ MHz, $A_2 = -25$ MHz, $A_{3,//[1,1,1]} = -40$ MHz, $\theta = 35.3^{\circ}$

A Tensor: nucleus ^{29}Si, spin $I = 1/2$, abundance 4.7%, 3 equivalent sites

$A_1 = -11$ MHz, $A_2 = -11$ MHz, $A_{3,//[1,1,1]} = -14$ MHz, $\theta = 35.3^{\circ}$

A Tensor: nucleus ^{29}Si, spin $I = 1/2$, abundance 4.7%, 3 equivalent sites

$A_1 = -6$ MHz, $A_2 = -6$ MHz, $A_{3,//[1,1,1]} = -8$ MHz, $\theta = 35.3^{\circ}$

Above 110 K

Symmetry: trigonal

Electron spin: $S = 1/2$

g tensor: $g_{//[1,1,1]} = 2.0081$, $g_{\perp[1,1,1]} = 2.0064$

Model: hydrogen atom saturating dangling bond of vacancy, neutral charge state, monoclinic symmetry below 45 K, above 110 K in motionally averaged state with trigonal symmetry, anneals out at $T = 200$ °C

References: 6, 52, 188, 189

Spectrum/model: Si-S1$_a$/(V$_2$H)^0

Symmetry: monoclinic-I

Electron spin: $S = 1/2$

g Tensor: $g_1 = 2.0110$, $g_{2,//[0,1,1]} = 2.0100$, $g_3 = 2.0008$, $\theta = 31.0°$

A Tensor: nucleus ^{1}H, spin $I = 1/2$, abundance 100%, 1 site

$A_1 = 1.4$ MHz, $A_{2,//[0,1,1]} = 1.6$ MHz, $A_3 = 3.8$ MHz, $\theta = 4.5°$

A Tensor: nucleus ^{29}Si, spin $I = 1/2$, abundance 4.7%, 1 site, trigonal within error limits

$A_1 = -268$ MHz, $A_2 = -268$ MHz, $A_{3,//[1,1,1]} = -420$ MHz, $\theta = 35.3°$

A Tensor: nucleus ^{29}Si, spin $I = 1/2$, abundance 4.7%, 2 equivalent sites

$A_1 = -41$ MHz, $A_2 = -41$ MHz, $A_{3,//[1,1,1]} = -48$ MHz, $\theta = 35.3°$

A Tensor: nucleus ^{29}Si, spin $I = 1/2$, abundance 4.7%, 3 equivalent sites

$A_1 = -22.5$ MHz, $A_2 = -22.5$ MHz, $A_{3,//[1,1,1]} = -36.5$ MHz, $\theta = 35.3°$

Model: hydrogen atom saturating dangling bond in di-vacancy, neutral charge state, anneals out at $T = 250$ °C

References: 6

Spectrum/model: Si-S1$_b$/(V$_3$H)^0

Symmetry: monoclinic-I

Electron spin: $S = 1/2$

g Tensor: $g_1 = 2.0100$, $g_{2,//[0,1,1]} = 2.0094$, $g_3 = 2.0009$, $\theta = 33.2°$

A Tensor: nucleus ^{29}Si, spin $I = 1/2$, abundance 4.7%, 1 site, trigonal within error limits

$A_1 = -261$ MHz, $A_2 = -261$ MHz, $A_{3,//[1,1,1]} = -420$ MHz, $\theta = 35.3°$

A Tensor: nucleus ^{29}Si, spin $I = 1/2$, abundance 4.7%, 2 equivalent sites

$A_1 = -37$ MHz, $A_2 = -37$ MHz, $A_{3,//[1,1,1]} = -43$ MHz, $\theta = 35.3°$

A Tensor: nucleus ^{29}Si, spin $I = 1/2$, abundance 4.7%, 3 equivalent sites

$A_1 = -23.0$ MHz, $A_2 = -23.0$ MHz, $A_{3,//[1,1,1]} = -32.5$ MHz, $\theta = 35.3°$

Model: hydrogen atom saturating dangling bond in tri-vacancy (or in tetra-vacancy), neutral charge state, anneals out at $T = 250$ °C

References: 6

Spectrum/model: Si-HVH/(H$_2$V)^0

Symmetry: orthorhombic-I

Electron spin: $S = 1$

g Tensor: $g_{[1,0,0]} = 2.002$, $g_{[0,1,1]} = 2.005$, $g_{[0,-1,1]} = 2.002$

D Tensor: $D_{[1,0,0]} = 348$ MHz, $D_{[0,1,1]} = 302$ MHz, $D_{[0,-1,1]} = 650$ MHz

A Tensor: nucleus ^{1}H, spin $I = 1/2$, abundance 100%, 2 sites

$A_{[1,0,0]} = 5.80$ MHz, $A_{[0,1,1]} = 5.32$ MHz, $A_{[0,-1,1]} = 6.29$ MHz

A Tensor: nucleus ^{29}Si, spin $I = 1/2$, abundance 4.7%, 2 sites, trigonal within error limits
$A_{//[1,1,1]} = -220$ MHz, $A_{\perp[1,1,1]} = -114$ MHz
Model: neutral di-hydrogen–vacancy complex in excited spin-triplet state
References: 55, 60 – 62

Spectrum/model: VOH^0

Below 180 K
Symmetry: monoclinic-I
Electron spin: $S = 1/2$
g Tensor: $g_{//[0,1,1]} = 2.0086$, $g_{\perp[0,1,1]} = 2.0084$, $g_{\perp[0,1,1]} = 2.0013$, $\theta = 39.2°$
A Tensor: nucleus ^{1}H, spin $I = 1/2$, abundance 100%, 1 site
$A_{//[0,1,1]} = -0.3$ MHz, $A_{\perp[0,1,1]} = -0.8$ MHz, $A_{\perp[0,1,1]} = 15.2$ MHz, $\theta = 1.0°$
A Tensor: nucleus ^{29}Si, spin $I = 1/2$, abundance 4.7%, 1 site, trigonal within error limits
$A_1 = -236$ MHz, $A_2 = -236$ MHz, $A_{3,//[1,1,1]} = -418$ MHz, $\theta = 35.3°$
Model: mono-vacancy–oxygen complex binding one hydrogen atom
Above 240 K
Symmetry: orthorhombic-I
Electron spin: $S = 1/2$
g Tensor: $g_{//[0,1,1]} = 2.0087$, $g_{\perp[0,1,1]} = 2.0057$, $g_{\perp[0,1,1]} = 2.0043$, $\theta = 39.2°$
A Tensor: nucleus ^{1}H, spin $I = 1/2$, abundance 100%, 1 site
$A_{//[0,1,1]} = -0.5$ MHz, $A_{\perp[0,1,1]} = -0.6$ MHz, $A_{\perp[0,1,1]} = 14.6$ MHz, $\theta = 0°$
Model: motionally averaged state of VOH
References: 63

Spectrum/model: Si-NL10/TDD(H,Al), D(N,O), heat treatment

Symmetry: orthorhombic-I (monoclinic-I, triclinic)
Electron spin: $S = 1/2$
g Tensor: $g_1 = 1.99959$, $g_2 = 1.99747$, $g_3 = 1.99957$, stage NL10
$g_1 = 1.99974$, $g_2 = 1.99770$, $g_3 = 1.99949$, stage NL13
$g_1 = 1.99982$, $g_2 = 1.99799$, $g_3 = 1.99946$, stage NL17
$g_1 = 1.99978$, $g_2 = 1.99765$, $g_3 = 1.99941$, species 1
$g_1 = 1.99978$, $g_2 = 1.99779$, $g_3 = 1.99941$, species 2
$g_1 = 1.99978$, $g_2 = 1.99793$, $g_3 = 1.99941$, species 3
$g_1 = 1.99978$, $g_2 = 1.99797$, $g_3 = 1.99941$, species 4
$g_1 = 1.99978$, $g_2 = 1.99813$, $g_3 = 1.99941$, species 5
A Tensor: oxygen ^{17}O, see Refs 75, 80, 84, 191 – 193
silicon ^{29}Si, see Refs 82, 86
aluminium ^{27}Al, see Refs 75, 80, 88, 194 – 197
hydrogen ^{1}H, see Refs 75, 97, 104, 198 – 200

Remarks: superposition of several component spectra, overall g tensor dependent on heat-treatment time, spectra with original labels NL13 and NL17 correspond to later annealing stages of NL10, g tensor given in orthorhombic approximation, actual symmetry may be lower
Model: neutral hydrogen-passivated thermal double donor, $(TDD\text{-}H)^0$
References: 40, 75, 76, 78 – 80, 82 – 86, 88, 89, 92, 94 – 97, 99, 103 – 107, 191 – 213

Spectrum/model: Si-NL10*/heat treatment
Symmetry: cubic
Electron spin: $S = 1/2$
g Tensor: $g = 1.999$
References: 95

Spectrum/model: Si-TU1/H,O-related centre
Symmetry: cubic
Electron spin: $S = 1/2$
g Tensor: $g = 1.9987$
A Tensor: nucleus ^{29}Si, spin $I = 1/2$, abundance 4.7%, 1 site: $A = 60$ MHz
Model: hydrogen–oxygen-related negative-U donor centre
References: 98, 99

Spectrum/model: Si-NL54/$(S_sH_i)^0$
Symmetry: trigonal
Electron spin: $S = 1/2$
g Tensor: $g_{//[1,1,1]} = 1.99886$, $g_{\perp[1,1,1]} = 2.00126$
A Tensor: nucleus ^1H, spin $I = 1/2$, abundance 100%, 1 site
$A_{//[1,1,1]} = 6.281$ MHz, $A_{\perp[1,1,1]} = 3.936$ MHz
A and Q Tensor: deuterium ^2H, spin $I = 1$, enrichment 100%, 1 site
$A_{//[1,1,1]} = 0.959$ MHz, $A_{\perp[1,1,1]} = 0.591$ MHz
$Q_{//[1,1,1]} = 0.048$ MHz, $Q_{\perp[1,1,1]} = -0.024$ MHz
A and Q Tensor: sulphur ^{33}S, spin $I = 3/2$, enrichment 25.54%, 1 site
$A_{//[1,1,1]} = 143.1$ MHz, $A_{\perp[1,1,1]} = 137.7$ MHz
$Q_{//[1,1,1]} = 6.6$ MHz, $Q_{\perp[1,1,1]} = -3.3$ MHz
Model: neutral trigonal substitutional-sulphur–interstitial-hydrogen pair
References: 111, 112, 200, 214 – 217

Spectrum/model: Si-NL55/$(S_sH_i)^0$
Symmetry: trigonal
Electron spin: $S = 1/2$

g Tensor: $g_{//[1,1,1]} = 1.99823$, $g_{\perp[1,1,1]} = 1.99974$
A Tensor: nucleus ^{1}H, spin $I = 1/2$, abundance 100%, 1 site
$A_{//[1,1,1]} = 5.801$ MHz, $A_{\perp[1,1,1]} = 5.500$ MHz
A and Q Tensor: deuterium ^{2}H, spin $I = 1$, enrichment 100%, 1 site
$A_{//[1,1,1]} = 0.867$ MHz, $A_{\perp[1,1,1]} = 0.823$ MHz
$Q_{//[1,1,1]} = 0.038$ MHz, $Q_{\perp[1,1,1]} = -0.019$ MHz
A and Q Tensor: sulphur ^{33}S, spin $I = 3/2$, enrichment 25.54%, 1 site
$A_{//[1,1,1]} = 124.0$ MHz, $A_{\perp[1,1,1]} = 117.9$ MHz
$Q_{//[1,1,1]} = 5.0$ MHz, $Q_{\perp[1,1,1]} = -2.5$ MHz
Model: neutral trigonal substitutional-sulphur–interstitial-hydrogen pair
References: 111, 112, 200, 214 – 217

Spectrum/model: Si-NL60/$(Se_sH_i)^0$
Symmetry: trigonal
Electron spin: $S = 1/2$
g Tensor: $g_{//[1,1,1]} = 1.99635$, $g_{\perp[1,1,1]} = 1.99459$
A Tensor: nucleus ^{1}H, spin $I = 1/2$, abundance 100%, 1 site
$A_{//[1,1,1]} = 6.782$ MHz, $A_{\perp[1,1,1]} = 6.603$ MHz
A and Q Tensor: deuterium ^{2}H, spin $I = 1$, enrichment 100%, 1 site
$A_{//[1,1,1]} = 1.017$ MHz, $A_{\perp[1,1,1]} = 0.990$ MHz
$Q_{//[1,1,1]} = -0.032$ MHz, $Q_{\perp[1,1,1]} = 0.016$ MHz
A Tensor: selenium ^{77}Se, spin $I = 1/2$, enrichment 99.1%, 1 site
$A_{//[1,1,1]} = 535.6$ MHz, $A_{\perp[1,1,1]} = 495.3$ MHz
Model: neutral trigonal substitutional-selenium–interstitial-hydrogen pair
References: 112, 216, 218

Spectrum/model: Si-NL61/$[Se_s(H_i)_2]^0$
Symmetry: trigonal
Electron spin: $S = 1/2$
g Tensor: $g_{//[1,1,1]} = 1.99627$, $g_{\perp[1,1,1]} = 1.99512$
A Tensor: nucleus ^{1}H, spin $I = 1/2$, abundance 100%, 1 site
$A_{//[1,1,1]} = 1.060$ MHz, $A_{\perp[1,1,1]} = 0.816$ MHz
A Tensor: nucleus ^{1}H, spin $I = 1/2$, abundance 100%, 1 site
$A_{//[1,1,1]} = 1.020$ MHz, $A_{\perp[1,1,1]} = 0.735$ MHz
A Tensor: selenium ^{77}Se, spin $I = 1/2$, enrichment 99.1%, 1 site
$A_{//[1,1,1]} = 321.5$ MHz, $A_{\perp[1,1,1]} = 296.8$ MHz
Model: neutral trigonal complex of substitutional selenium and two inequivalent interstitial hydrogen atoms
References: 112, 216, 218

Spectrum/model: $[Pt_s(H_i)_2]^-$

Symmetry: orthorhombic-I

Electron spin: $S = 1/2$

g Tensor: for PtH_2: $g_{//[1,0,0]} = 2.1298$, $g_{//[0,1,1]} = 1.9558$, $g_{//[0,-1,1]} = 2.1683$

for PtD_2: $g_{//[1,0,0]} = 2.1319$, $g_{//[0,1,1]} = 1.9554$, $g_{//[0,-1,1]} = 2.1688$

A Tensor: nucleus ^{195}Pt, spin $I = 1/2$, natural abundance 33%, 1 site

for PtH_2: $A_{//[1,0,0]} = 175.7$ MHz, $A_{//[0,1,1]} = 541.2$ MHz, $A_{//[0,-1,1]} = 237.3$ MHz

for PtD_2: $A_{//[1,0,0]} = 182.5$ MHz, $A_{//[0,1,1]} = 545.8$ MHz, $A_{//[0,-1,1]} = 239.9$ MHz

A Tensor: nucleus ^1H, spin $I = 1/2$, natural abundance 100%, 2 sites

$A_{//[1,0,0]} \approx 9.8$ MHz, $A_{//[0,1,1]} \approx 7.9$ MHz, $A_{//[0,-1,1]} \approx 8.2$ MHz

A Tensor: nucleus ^{29}Si, spin $I = 1/2$, natural abundance 4.7%, 2 sites

$A_{//[1,1,1]} \approx 124$ MHz, $A_{\perp[1,1,1]} \approx 88$ MHz

Model: platinum atom bridging two dangling bonds in vacancy, two hydrogen atoms terminating other two bonds in same vacancy

References: 3, 4, 116, 117, 219, 220

Spectrum/model: Si-NL53/$[Pt_s(H_i)_2]_3$

Symmetry: trigonal

Electron spin: $S = 1/2$

g Tensor: $g_{//[1,1,1]} = 2.5082$, $g_{\perp[1,1,1]} = 2.0206$

A Tensor: nucleus ^{195}Pt, spin $I = 1/2$, natural abundance 33%

$A_{\perp[0,1,1]} = 327.3$ MHz, $A_{//[0,1,1]} = 432.7$ MHz, $A_{\perp[0,1,1]} = 349.4$ MHz, $\theta = 12.4^\circ$

Model: see Fig. 8 of Ref. 3

References: 3, 219

Spectrum/model: Si-NL64/$Au_s(H_i)_1(H_i)_2$

Symmetry: triclinic

Electron spin: $S = 1/2$

g Tensor: $g_{xx} = 2.1282$, $g_{yy} = 2.0690$, $g_{zz} = 2.0039$

$g_{xy} = -0.0732$, $g_{yz} = 0.0394$, $g_{zx} = 0.0361$

A Tensor: nucleus ^{197}Au, spin $I = 3/2$, natural abundance 100%, 1 site

$A_{xx} = 13.8$ MHz, $A_{yy} = 23.5$ MHz, $A_{zz} = 18.1$ MHz

$A_{xy} = 8.72$ MHz, $A_{yz} = -6.36$ MHz, $A_{zx} = 1.06$ MHz

A Tensor nucleus ^1H, spin $I = 1/2$, natural abundance 100%, 2 sites

$A_{xx} = 8.68$ MHz, $A_{yy} = 11.39$ MHz, $A_{zz} = 8.54$ MHz

$A_{xy} = 1.73$ MHz, $A_{yz} = -0.24$ MHz, $A_{zx} = 0.14$ MHz

Model: substitutional-gold–two-interstitial-hydrogen centre, see Fig. 4 of Ref. 125

References: 125 – 127

Spectrum/model: Si-NL65/$[Pt_s(H_i)_3]^0$

Symmetry: trigonal

Electron spin: $S = 1/2$

g Tensor: $g_{//[1,1,1]} = 1.9673$, $g_{\perp[1,1,1]} = 2.1569$

A Tensor: nucleus ^1H, spin $I = 1/2$, abundance 100%, 3 sites

$A_{//} = 14.5$ MHz, $A_{\perp} = 12.7$ MHz

A Tensor: selenium ^{195}Pt, spin $I = 1/2$, abundance 33%, 1 site

$A_{//} = 708.8$ MHz, $A_{\perp} = 52.2$ MHz

Model: neutral trigonal substitutional-platinum–three-interstitial-hydrogen centre

References: 125 – 127

Spectrum/model: FeH

Symmetry: cubic

Electron spin: $S = 1/2$

g Tensor: $g \approx 2.07$

References: 146

Spectrum/model: Si-AA17

Symmetry: trigonal

Electron spin: $S = 1$

g Tensor: $g_{//[1,1,1]} = 2.0028$, $g_{\perp[1,1,1]} = 2.0106$

D Tensor: $D_{//[1,1,1]} = \pm 33.6$ MHz, $D_{\perp[1,1,1]} = \pm 16.8$ MHz

A Tensor: nucleus ^{29}Si, spin $I = 1/2$, abundance 4.7%, 2 sites

$A_{//[1,1,1]} = \pm 175$ MHz, $A_{\perp[1,1,1]} = \pm 89$ MHz

Model: hexa-vacancy ring, two hydrogen atoms on equivalent positions above and below ring, neutral state

References: 147, 151

Spectrum/model: Si-AA15/Al_i–Al_i–H

Symmetry: monoclinic-I

Electron spin: $S = 1/2$

g Tensor: $g_{//[0,1,1]} = 2.0025$, $g_{\perp[0,1,1]} = 2.0035$, $g_{\perp[0,1,1]} = 2.0008$, $\theta = 70°$

A Tensor: nucleus ^{27}Al, spin $I = 5/2$, abundance 100, 1 site

$A_{//[0,1,1]} = 318.0$ MHz, $A_{\perp[0,1,1]} = 290.1$ MHz, $A_{\perp[0,1,1]} = 276.8$ MHz, $\theta = 20°$

A Tensor: nucleus ^{27}Al, spin $I = 5/2$, abundance 100, 1 site

$A_{//[0,1,1]} = 285.5$ MHz, $A_{\perp[0,1,1]} = 277.5$ MHz, $A_{\perp[0,1,1]} = 267.3$ MHz, $\theta = 33°$

Model: Al_i–Al_i <110> split interstitial, H on nearby interstitial site, anneals in at 200 K, anneals out at 300 K

References: 7, 161 – 164, 221

Spectrum/model: Si-AA16/Al_i–H

Symmetry: nearly isotropic
Electron spin: $S = 1/2$
g Tensor: $g = 2.0035$
A Tensor: nucleus ^{27}Al, spin $I = 5/2$, abundance 100, 1 site
$A_{//[1,1,1]} = 823$ MHz, $A_{\perp[1,1,1]} = 836$ MHz
Model: interstitial Al_i, H on nearby BC site, anneals in at 180 K, anneals out at 210 K
References: 7, 162 – 164, 221

Spectrum/model: Si-P_b

Symmetry: trigonal
Electron spin: $S = 1/2$
g Tensor: $g_{//[1,1,1]} = 2.0016$, $g_{\perp[1,1,1]} = 2.0090$ (Ref. 169)
$g_{//[1,1,1]} = 2.0011$, $g_{\perp[1,1,1]} = 2.0080$ (Ref. 170)
A Tensor: nucleus ^{29}Si, spin $I = 1/2$, abundance 4.7%, 1 site
$A_{//} = 438$ MHz, $A_{\perp} = 255$ MHz (Ref. 169)
$A_{//} = 423$ MHz, $A_{\perp} = 234$ MHz (Ref. 170)
A Tensor: nucleus ^{1}H, spin $I = 1/2$, abundance 100%, 6 sites
$A_{//} = 380$ kHz, $A_{\perp} = 248$ kHz
A Tensor: nucleus ^{1}H, spin $I = 1/2$, abundance 100%, 6 sites
$A_{//} = 201$ kHz, $A_{\perp} = 142$ kHz
A Tensor: nucleus ^{1}H, spin $I = 1/2$, abundance 100%, 12 sites
$A_{//} = 110$ kHz, $A_{\perp} = 84$ kHz
Model: neutral dangling bond on (111) Si/SiO_2 interface, $(–Si{\equiv}Si_3)^0$
References: 165 – 173, 175, 222 – 226

Spectrum/model: Si-NL52

Symmetry: trigonal
Electron spin: $S = 1/2$
g Tensor: $g_{//[1,1,1]} = 2.00069$, $g_{\perp[1,1,1]} = 2.00951$
A Tensor: nucleus ^{29}Si, spin $I = 1/2$, abundance 4.7%, 1 site
$A_{//} = 436$ MHz, $A_{\perp} = 256$ MHz
A Tensor: nucleus ^{1}H, spin $I = 1/2$, abundance 100%
$A_{//} = 4.8$ MHz, $A_{\perp} = 1.5$ MHz
A Tensor: nucleus ^{1}H, spin $I = 1/2$, abundance 100%
$A_{//} = 12.1$ MHz, $A_{\perp} = -5.0$ MHz
Model: P_b-like centre decorated with hydrogen
References: 7, 174, 177, 180, 227 – 230

References

Books and review articles

"Hydrogen in Crystalline Semiconductors", S. J. Pearton, J. W. Corbett and T. S. Shi, Appl. Phys. A 43 (1987) pp. 153–195

"Hydrogen in Semiconductors", edited by J. I. Pankove and N. M. Johnson, Semiconductors and Semimetals 34 (1991)

"Hydrogen in Semiconductors: Bulk and Surface Properties", edited by M. Stutzmann and J. Chevallier, Physica B 170 (1991) pp. 1–581

"Hydrogen Interactions with Defects in Crystalline Solids", S. M. Myers, M. I. Baskes, H. K. Birnbaum, J. W. Corbett, G. G. DeLeo, S. K. Estreicher, E. E. Haller, P. Jena, N. M. Johnson, R. Kirchheim, S. J. Pearton and M. J. Stavola, Rev. Mod. Phys. 64 (1992) pp. 559–617

"Hydrogen in Crystalline Semiconductors", S. J. Pearton, J. W. Corbett and M. Stavola, (Springer-Verlag, Berlin, 1992), pp. 1–363

"Hydrogen in Semiconductors and Metals", edited by N. H. Nickel, W. B. Jackson, R. C. Bowman and R. G. Leisure, Mat. Res. Soc. Symp. Proc. Vol. 513 (Materials Research Society, Warrendale, 1998), pp. 1–455

"Hydrogen in Semiconductors II", edited by N. H. Nickel, Semiconductors and Semimetals 61 (1999) pp. 1–508

"Hydrogen Diffusion and Solubility in c-Si" in EMIS Datareviews Series No. 20, M. Stavola, (INSPEC, IEE, London, 1999) pp. 511–521

"Hydrogen-Containing Point defects in c-Si" in EMIS Datareviews Series No. 20, M. Stavola, (INSPEC, IEE, London, 1999) pp. 522–537

"Defects in Silicon: Hydrogen", edited by J. Weber and A. Mesli, Mater. Sci. Eng. B 58 (1999) pp. 1–183

"The Interaction of Hydrogen with Deep Level Defects in Silicon", R. Jones, B. J. Coomer, J. P. Goss, B. Hourahine and A. Resende, Solid State Phenom. 71 (2000) pp. 173–248

Articles

[1] A. van Wieringen and N. Warmoltz, Physica 22 (1956) pp. 849–865

[2] D. J. Fisher, editor, Defect Diffus. Forum 153–155 (1998) pp. 1–555

[3] M. Höhne, U. Juda, Yu. V. Martynov, T. Gregorkiewicz, C. A. J. Ammerlaan and L. S. Vlasenko, Phys. Rev. B 49 (1994) pp. 13423–13429

[4] S. J. Uftring, M. Stavola, P. M. Williams and G. D. Watkins, Phys. Rev. B 51 (1995) pp. 9612–9621

[5] H. Lütgemeier and K. Schnitzke, Phys. Lett. 25A (1967) pp. 232–233

[6] P. Stallinga, P. Johannesen, S. Herstrøm, K. Bonde Nielsen, B. Bech Nielsen and J. R. Byberg, Phys. Rev. B 58 (1998) pp. 3842–3852

[7] Yu. V. Gorelkinskii, Semiconductors and Semimetals 61 (1999) pp. 25–81

[8] J. Weber and D. I. Bohne, Early Stages of Oxygen Precipitation in Silicon (Kluwer Academic Publishers, Dordrecht, 1996) pp. 123–140

[9] Y. Kamiura, N. Ishiga and Y. Yamashita, Jpn. J. Appl. Phys. 36 (1997) pp. L1419–L1421

[10] N. Yarykin, J.–U. Sachse, H. Lemke and J. Weber, Phys. Rev. B 59 (1999) pp. 5551–5560

[11] G. Pensl, G. Roos, P. Stolz, N. M. Johnson and C. Holm, Defects in Electronic Materials (Materials Research Society, Pittsburgh, 1988) pp. 241–246

[12] Y. Ohmura, K. Takahashi, H. Saitoh, T. Kon and A. Enosawa, Physica B 273–274 (1999) pp. 228–230

[13] J. I. Pankove, D. E. Carlson, J. E. Berkeyheiser and R. O. Wance, Phys. Rev. Lett. 51 (1983) pp. 2224–2225

[14] C.–T. Sah, Jack Y.–C. Sun and Joseph J.–T. Tzou, Appl. Phys. Lett. 43 (1983) pp. 204–206

[15] P. J. H. Denteneer, C. G. Van de Walle and S. T. Pantelides, Phys. Rev. B 39 (1989) pp. 10809–10824

[16] N. M. Johnson, C. Herring and D. J. Chadi, Phys. Rev. Lett. 56 (1986) pp. 769–772

[17] L. Hoffmann, E. V. Lavrov and B. Bech Nielsen, Mater. Sci. Eng. B 58 (1999) pp. 167–170

[18] Yu. V. Gorelkinskii and N. N. Nevinnyi, Sov. Tech. Phys. Lett. 13 (1987) pp. 45–46 [Pis'ma Zh. Tekh. Fiz. (USSR) 13 (1987) pp. 105–109]

[19] Yu. V. Gorelkinskii and N. N. Nevinnyi, Physica B 170 (1991) pp. 155–167

[20] K. W. Blazey, T. L. Estle, E. Holzschuh, W. Odermatt and B. D. Patterson, Phys. Rev. B 27 (1983) pp. 15–19

[21] C. G. Van de Walle and P. E. Blöchl, Phys. Rev. B 47 (1993) pp. 4244–4255

[22] R. F. Kiefl, M. Celio, T. L. Estle, S. R. Kreitzman, G. M. Luke, T. M. Riseman and E. J. Ansaldo, Phys. Rev. Lett. 60 (1988) pp. 224–226

[23] G. D. Watkins and J. W. Corbett, Phys. Rev. 134 (1964) pp. A1359–A1377

[24] S. Estreicher, Phys. Rev. B 36 (1987) pp. 9122–9128

[25] C. G. Van de Walle, P. J. H. Denteneer, Y. Bar–Yam and S. T. Pantelides, Phys. Rev. B 39 (1989) pp. 10791–10808
[26] Yu. V. Gorelkinskii and N. N. Nevinnyi, Mater. Sci. Eng. B 36 (1996) pp. 133–137
[27] K. Irmscher, H. Klose and K. Maass, J. Phys. C: Solid State Phys. 17 (1984) pp. 6317–6329
[28] B. Holm, K. Bonde Nielsen and B. Bech Nielsen, Phys. Rev. Lett. 66 (1991) pp. 2360–2363
[29] B. Bech Nielsen, K. Bonde Nielsen and J. R. Byberg, Mater. Sci. Forum 143–147 (1994) pp. 909–913
[30] P. Deák, L. C. Snyder, J. L. Lindström, J. W. Corbett, S. J. Pearton and A. J. Tavendale, Phys. Lett. A 126 (1988) pp. 427–430
[31] C. G. Van de Walle, Physica B 170 (1991) pp. 21–32
[32] K. J. Chang and D. J. Chadi, Phys. Rev. B 40 (1989) pp. 11644–11653
[33] N. M. Johnson, C. Herring and C. G. Van de Walle, Phys. Rev. Lett. 73 (1994) pp. 130–133
[34] Yu. V. Gorelkinskii, V. O. Sigle and Zh. S. Takibaev, Phys. Status Solidi (a) 22 (1974) pp. K55–K57
[35] Yu. V. Gorelkinskii, N. N. Nevinnyi and S. S. Ajazbaev, Phys. Lett. A 125 (1987) pp. 354–358
[36] Yu. V. Gorelkinskii and N. N. Nevinnyi, Radiat. Eff. 71 (1983) pp. 1–8
[37] Yu. Gorelkinskii and N. N. Nevinnyi, Nucl. Instrum. Methods 209–210 (1983) pp. 677–682
[38] J. Hartung and J. Weber, Phys. Rev. B 48 (1993) pp. 14161–14166
[39] J. Hartung and J. Weber, J. Appl. Phys. 77 (1995) pp. 118–121
[40] S. H. Muller, M. Sprenger, E. G. Sieverts and C. A. J. Ammerlaan, Solid State Commun. 25 (1978) pp. 987–990
[41] R. Dirksen, F. Berg Rasmussen, T. Gregorkiewicz and C. A. J. Ammerlaan, Mater. Sci. Forum 258–263 (1997) pp. 373–378
[42] Yu. V. Gorelkinskii, N. N. Nevinnyi and Kh. A. Abdullin, J. Appl. Phys. 84 (1998) pp. 4847–4850
[43] J. M. Trombetta, G. D. Watkins, J. Hage and P. Wagner, J. Appl. Phys. 81 (1997) pp. 1109–1115
[44] P. Stallinga, T. Gregorkiewicz, C. A. J. Ammerlaan and Yu. V. Gorelkinskii, Solid State Commun. 90 (1994) pp. 401–404
[45] D. F. Daly, J. Appl. Phys. 42 (1971) pp. 864–865
[46] K. L. Brower, Phys. Rev. B 14 (1976) pp. 872–883
[47] Yu. V. Gorelkinskii and N. N. Nevinnyi, Phys. Lett. 99A (1983) pp. 117–120
[48] Yu. V. Gorelkinskii and N. N. Nevinnyi, Proc. 7th Int. Conf. on Ion Implantation in Semiconductors and Other Materials, Vilnius, 1983, pp. 59–60

[49] H. Lütgemeier and K. Schnitzke, Phys. Lett. 25A (1967) pp. 726–727
[50] V. A. Botvin, Yu. V. Gorelkinskii, V. O. Sigle and M. A. Chubisov, Sov. Phys. – Semicond. 6 (1973) pp. 1453–1456 [Fiz. Tekh. Poluprovodn. 6 (1973) pp. 1683–1686]
[51] A. V. Dvurechenskii and A. A. Karanovich, Sov. Phys. – Semicond. 19 (1985) pp. 1198–1200 [Fiz. Tekh. Poluprovodn. 19 (1985) pp. 1944–1948]
[52] B. Bech Nielsen, P. Johannesen, P. Stallinga, K. Bonde Nielsen and J. R. Byberg, Phys. Rev. Lett. 79 (1997) pp. 1507–1510
[53] D. F. Daly and K. A. Pickar, Appl. Phys. Lett. 15 (1969) pp. 267–269
[54] R. L. Kleinhenz, Y. H. Lee, V. A. Singh, P. M. Mooney, A. Jaworowski, L. M. Roth, J. C. Corelli and J. W. Corbett, Defects and Radiation Effects in Semiconductors 1978 (Institute of Physics, Bristol, 1979) pp. 200–204
[55] W. M. Chen, O. O. Awadelkarim, B. Monemar, J. L. Lindström and G. S. Oehrlein, Phys. Rev. Lett. 64 (1990) pp. 3042–3045
[56] K. L. Brower, Phys. Rev. B 4 (1971) pp. 1968–1982
[57] Hongqi Xu, Phys. Rev. B 46 (1992) pp. 1403–1422
[58] B. Bech Nielsen, L. Hoffmann, M. Budde, R. Jones, J. Goss and S. Öberg, Mater. Sci. Forum 196–201 (1995) pp. 933–937
[59] B. Bech Nielsen, L. Hoffmann and M. Budde, Mater. Sci. Eng. B 36 (1996) pp. 259–263
[60] P. Stallinga and B. B. Nielsen, Acta Phys. Pol. A 92 (1997) pp. 989–992
[61] P. Stallinga and B. Bech Nielsen, Phys. Rev. Lett. 80 (1998) p. 422
[62] W. M. Chen, O. O. Awadelkarim, B. Monemar, J. L. Lindström and G. S. Oehrlein Phys. Rev. Lett. 80 (1998) p. 423
[63] P. Johannesen, J. R. Byberg and B. Bech Nielsen, Physica B 273–274 (1999) pp. 180–183
[64] C. S. Fuller, J. A. Ditzenberger, N. B. Hannay and E. Buehler, Phys. Rev. 96 (1954) p. 833
[65] C. S. Fuller and R. A. Logan, J. Appl. Phys. 28 (1957) pp. 1427–1436
[66] W. Kaiser, H. L. Frisch and H. Reiss, Phys. Rev. 112 (1958) pp. 1546–1554
[67] P. Gaworzewski and K. Schmalz, Phys. Status Solidi (a) 55 (1979) pp. 699–707
[68] V. V. Emtsev, G. A. Oganesyan and K. Schmalz, Defect Diffus. Forum 103–105 (1993) pp. 505–516
[69] P. Wagner and J. Hage, Appl. Phys. A 49 (1989) pp. 123–138
[70] W. Götz, G. Pensl and W. Zulehner, Phys. Rev. B 46 (1992) pp. 4312–4315
[71] M. Tajima, S. Kishino, M. Kanamori and T. Iizuka, J. Appl. Phys. 51 (1980) pp. 2247–2254
[72] A. G. Steele and M. L. W. Thewalt, Can. J. Phys. 67 (1989) pp. 268–274
[73] J. L. Benton, K. M. Lee, P. E. Freeland and L. C. Kimerling, J. Electron. Mater. 14a (1985) pp. 647–652
[74] D. I. Bohne and J. Weber, Phys. Rev. B 47 (1993) pp. 4037–440
[75] C. A. J. Ammerlaan, I. S. Zevenbergen, Yu. V. Martynov and T. Gregorkiewicz, Early Stages of Oxygen Precipitation in Silicon (Kluwer, Dordrecht, 1996) pp. 61–82

[76] J.–M. Spaeth, Early Stages of Oxygen Precipitation in Silicon (Kluwer, Dordrecht, 1996) pp. 83–101

[77] R. Jones, editor, Early Stages of Oxygen Precipitation in Silicon (Kluwer Academic Publishers, Dordrecht, 1996) pp. 1–530

[78] T. Gregorkiewicz, D. A. van Wezep, H. H. P. Th. Bekman and C. A. J. Ammerlaan, Phys. Rev. B 35 (1987) pp. 3810–3817

[79] S. H. Muller, E. G. Sieverts and C. A. J. Ammerlaan, Defects and Radiation Effects in Semiconductors, 1978 (Institute of Physics, Bristol, 1979) pp. 297–302

[80] T. Gregorkiewicz, H. H. P. Th. Bekman and C. A. J. Ammerlaan, Phys. Rev. B 38 (1988) pp. 3998–4015

[81] E. G. Sieverts, Phys. Status Solidi (b) 120 (1983) pp. 11–29

[82] C. A. J. Ammerlaan, T. Gregorkiewicz and H. H. P. Th. Bekman, Shallow Impurities in Semiconductors 1988 (Institute of Physics, Bristol, 1989) pp 191–200

[83] T. Gregorkiewicz, H. H. P. Th. Bekman, C. A. J. Ammerlaan, W. Knap, L. C. Brunel and G. Martinez, Phys. Rev. B 45 (1992) pp. 5873–5878

[84] T. Gregorkiewicz, D. A. van Wezep, H. H. P. Th. Bekman and C. A. J. Ammerlaan, Phys. Rev. Lett. 59 (1987) pp. 1702–1705

[85] J. Michel, J. R. Niklas and J.–M. Spaeth, Phys. Rev. B 40 (1989) pp. 1732–1747

[86] H. H. P. Th. Bekman, T. Gregorkiewicz and C. A. J. Ammerlaan, Phys. Rev. B 39 (1989) pp. 1648–1658

[87] K. M. Lee, J. M. Trombetta and G. D. Watkins, Microscopic Identification of Electronic Defects in Semiconductors (Materials Research Society, Pittsburgh, 1985) pp 263–268

[88] T. Gregorkiewicz, H. H. P. Th. Bekman and C. A. J. Ammerlaan, Phys. Rev. B 46 (1992) pp. 4582–4589

[89] J. Michel, N. Meilwes and J.–M. Spaeth, Phys. Rev. B 39 (1989) pp. 7978–7981

[90] M. Suezawa, K. Sumino and M. Iwaizumi, J. Appl. Phys. 54 (1983) pp. 6594–6600

[91] R. Wörner and O. F. Schirmer, Phys. Rev. B 34 (1986) pp. 1381–1383

[92] H. H. P. Th. Bekman, T. Gregorkiewicz, D. A. van Wezep and C. A. J. Ammerlaan, J. Appl. Phys. 62 (1987) pp. 4404–4405

[93] A. Hara, T. Fukuda, T. Miyabo and I. Hirai, Jpn. J. Appl. Phys. 28 (1989) pp. 142–143

[94] A. Hara, I. Hirai and A. Ohsawa, J. Appl. Phys. 67 (1990) pp. 2462–2465

[95] A. Hara, M. Aoki, M. Koizuka and T. Fukuda, J. Appl. Phys. 75 (1994) pp. 2929–2935

[96] A. Hara, M. Aoki, T. Fukuda and A. Ohsawa, Mater. Sci. Forum 117–118 (1993) pp. 219–224

[97] Yu. V. Martynov, T. Gregorkiewicz and C. A. J. Ammerlaan, Phys. Rev. Lett. 74 (1995) pp. 2030–2033

[98] V. P. Markevich, T. Mchedlidze and M. Suezawa, Phys. Rev. B 56 (1997) pp. R12695–R12697

[99] V. P. Markevich, T. Mchedlidze, M. Suezawa and L. I. Murin, Phys. Status Solidi (b) 210 (1998) pp. 545–549

[100] R. Murray, A. R. Brown and R. C. Newman, Mater. Sci. Eng. B 4 (1989) pp. 299–302

[101] S. K. Estreicher, Phys. Rev. B 41 (1990) pp. 9886–9891

[102] N. M. Johnson, S. K. Hahn and H. J. Stein, Mater. Sci. Forum 10–12 (1986) pp. 585–590

[103] I. S. Zevenbergen, Yu. V. Martynov, F. Berg Rasmussen, T. Gregorkiewicz and C. A. J. Ammerlaan, Mater. Sci. Eng. B 36 (1996) pp. 138–141

[104] Yu. V. Martynov, T. Gregorkiewicz and C. A. J. Ammerlaan, Mater. Sci. Forum 196–201 (1995) pp. 849–853

[105] R. C. Newman, M. J. Ashwin, R. E. Pritchard, J. H. Tucker, E. C. Lightowlers, T. Gregorkiewicz, I. S. Zevenbergen, C. A. J. Ammerlaan, R. Falster and M. J. Binns, Mater. Sci. Forum 258–263 (1997) pp. 379–384

[106] R. E. Pritchard, M. J. Ashwin, J. H. Tucker, R. C. Newman, E. C. Lightowlers, T. Gregorkiewicz, I. S. Zevenbergen, C. A. J. Ammerlaan, R. Falster and M. J. Binns, Semicond. Sci. Technol. 12 (1997) pp. 1404–1408

[107] R. C. Newman, J. H. Tucker, N. G. Semaltianos, E. C. Lightowlers, T. Gregorkiewicz, I. S. Zevenbergen and C. A. J. Ammerlaan, Phys. Rev. B 54 (1996) pp. R6803–R6806

[108] H. G. Grimmeiss and E. Janzén, Deep Centers in Semiconductors (Gordon and Breach Science Publishers, New York, 1986) pp. 87–146

[109] G. Pensl, G. Roos, C. Holm, E. Sirtl and N. M. Johnson, Appl. Phys. Lett. 51 (1987) pp. 451–453

[110] R. E. Peale, K. Muro and A. J. Sievers, Mater. Sci. Forum 65–66 (1990) pp. 151–156

[111] I. S. Zevenbergen, T. Gregorkiewicz and C. A. J. Ammerlaan, Phys. Rev. B 51 (1995) pp. 16746–16749

[112] P. T. Huy, C. A. J. Ammerlaan, T. Gregorkiewicz and D. T. Don, Phys. Rev. B 61 (2000) pp. 7448–7458

[113] A. S. Yapsir, P. Deák, R. K. Singh, L. C. Snyder, J. W. Corbett and T.-M. Lu, Phys. Rev. B 38 (1988) pp. 9936–9940

[114] V. J. B. Torres, S. Öberg and R. Jones, Shallow-Level Centers in Semiconductors (World Scientific, Singapore, 1997) pp. 501–504

[115] A. Resende, private communication (1999)

[116] P. M. Williams, G. D. Watkins, S. Uftring and M. Stavola, Phys. Rev. Lett. 70 (1993) pp. 3816–3819

[117] M. Stavola, S. J. Uftring, M. J. Evans, P. M. Williams and G. D. Watkins, Defect and Impurity Engineered Semiconductors and Devices (Materials Research Society, Pittsburgh, 1995) pp. 341–352

[118] J.-U. Sachse, E. Ö. Sveinbjörnsson, W. Jost, J. Weber and H. Lemke, Phys. Rev. B 55 (1997) pp. 16176–16185

[119] J. Weber, Hydrogen in Semiconductors and Metals (Materials Research Society, Warrendale, 1998) pp. 345–356
[120] J.–U. Sachse, J. Weber and E. Ö. Sveinbjörnsson, Phys. Rev. B 60 (1999) pp. 1474–1476
[121] R. Jones, A. Resende, S. Öberg and P. R. Briddon, Mater. Sci. Eng. B 58 (1999) p. 113–117
[122] S. J. Pearton and E. E. Haller, J. Appl. Phys. 54 (1983) pp. 3613–3615
[123] M. Höhne and U. Juda, J. Appl. Phys. 72 (1992) pp. 3095–3101
[124] M. Höhne and U. Juda, Mater. Sci. Technol. 11 (1995) pp. 680–683
[125] P. T. Huy and C. A. J. Ammerlaan, Physica B 302–303 (2001) pp. 233–238
[126] P. T. Huy and C. A. J. Ammerlaan, Solid State Phenom. (2001)
[127] P. T. Huy and C. A. J. Ammerlaan, Physica B (2001)
[128] E. Ö. Sveinbjörnsson, G. I. Andersson and O. Engström, Phys. Rev. B 49 (1994) pp. 7801–7804
[129] E. Ö. Sveinbjörnsson and O. Engström, Phys. Rev. B 52 (1995) pp. 4884–4895
[130] L. Rubaldo, P. Deixler, I. D. Hawkins, J. Terry, D. K. Maude, J.–C. Portal, J. H. Evans–Freeman, L. Dobaczewski and A. R. Peaker, Mater. Sci. Eng. B 58 (1999) pp. 126–129
[131] H. Feichtinger and E. Sturm, Mater. Sci. Forum 143–147 (1994) pp. 111–115
[132] M. J. Evans, M. Stavola, M. G. Weinstein and S. J. Uftring, Mater. Sci. Eng. B 58 (1999) pp. 118–125
[133] A. Resende, R. Jones, S. Öberg and P. R. Briddon, Mater. Sci. Eng. B 58 (1999) pp. 146–148
[134] R. Jones, B. J. Coomer, J. P. Goss, B. Hourahine and A. Resende, Solid State Phenom. 71 (2000) pp. 173–248
[135] J.–U. Sachse, E. Ö. Sveinbjörnsson, N. Yarykin and J. Weber, Mater. Sci. Eng. B 58 (1999) pp. 134–140
[136] S. Knack, J. Weber and H. Lemke, Mater. Sci. Eng. B 58 (1999) pp. 141–145
[137] J.–U. Sachse, J. Weber and H. Lemke, Mater. Sci. Forum 258–263 (1997) pp. 307–312
[138] J. Weber, S. Knack and J.–U. Sachse, Physica B 273–274 (1999) pp. 429–432
[139] W. Jost and J. Weber, Phys. Rev. B 54 (1996) pp. R11038–R11041
[140] T. Sadoh, H. Nakashima and T. Tsurushima, J. Appl. Phys. 72 (1992) pp. 520–524
[141] T. Sadoh, M. Watanabe, H. Nakashima and T. Tsurushima, Mater. Sci. Forum 143–147 (1994) pp. 939–943
[142] W. Jost, J. Weber and H. Lemke, Semicond. Sci. Technol. 11 (1996) pp. 22–26
[143] W. Jost, J. Weber and H. Lemke, Semicond. Sci. Technol. 11 (1996) pp. 525–530
[144] M. Shiraishi, J.–U. Sachse, H. Lemke and J. Weber, Mater. Sci. Eng. B 58 (1999) pp. 130–133
[145] S. Knack, J. Weber and H. Lemke, Physica B 273–274 (1999) pp. 387–390
[146] T. Takahashi and M. Suezawa, Physica B 273–274 (1999) pp. 445–448

[147] Yu. V. Gorelkinskii, Kh. A. Abdullin and B. N. Mukashev, Physica B 273–274 (1999) pp. 171–175

[148] J. L. Hastings, S. K. Estreicher and P. A. Fedders, Phys. Rev. B 56 (1997) pp. 10215–10220

[149] A. N. Safonov, E. C. Lightowlers and G. Davies, Phys. Rev. B 56 (1997) pp. R15517–R15520

[150] A. N. Safonov and E. C. Lightowlers, Mater. Sci. Eng. B 58 (1999) pp. 39–47

[151] S. Zh. Tokmoldin, B. N. Mukashev, Kh. A. Abdullin and Yu. V. Gorelkinskii, Physica B 273–274 (1999) pp. 204–207

[152] V. A. Botvin, Yu. V. Gorelkinskii, V. A. Kudryashev and V. O. Sigle, Sov. Phys. – Semicond. 8 (1975) pp. 1049–1050 [Fiz. Tekh. Poluprovodn. 8 (1974) pp. 1614–1616]

[153] B. I. Vikhrev, N. N. Gerasimenko, A. V. Dvurechenskii and L. S. Smirnov, Sov. Phys. – Semicond. 8 (1975) pp. 871–872 [Fiz. Tekh. Poluprovodn. 8 (1974) pp. 1345–1348]

[154] R. C. Newman and R. Jones, Semiconductors and Semimetals 42 (1994) pp. 289–352

[155] J. W. Corbett, R. S. McDonald and G. D. Watkins, J. Phys. Chem. Solids 25 (1964) pp. 873–879

[156] R. Jones, S. Öberg and A. Umerski, Mater. Sci. Forum 83–87 (1992) pp. 551–561

[157] S. K. Estreicher, Y. K. Park and P. A. Fedders, Early Stages of Oxygen Precipitation in Silicon (Kluwer Academic Publishers, Dordrecht, 1996) pp. 179–195

[158] R. Murray, Physica B 170 (1991) pp. 115–123

[159] R. C. Newman, Early Stages of Oxygen Precipitation in Silicon (Kluwer Academic Publishers, Dordrecht, 1996) pp. 19–39

[160] R. C. Newman, Mater. Sci. Eng. B 36 (1996) pp. 1–12

[161] Yu. V. Gorelkinskii, Kh. A. Abdullin and B. N. Mukashev, Shallow-Level Centers in Semiconductors (World Scientific, Singapore, 1997) pp. 315–320

[162] Kh. A. Abdullin, B. N. Mukashev and Yu. V. Gorelkinskii, Appl. Phys. Lett. 71 (1997) pp. 1703–1705

[163] Yu. V. Gorelkinskii, B. N. Mukashev and Kh. A. Abdullin, Semiconductors 32 (1998) pp. 375–381 [Fiz. Tekh. Poluprovodn. 32 (1998) pp. 412–428]

[164] B. N. Mukashev, Kh. A. Abdullin, Yu. V. Gorelkinskii and S. Zh. Tokmoldin, Mater. Sci. Eng. B 58 (1999) pp. 171–178

[165] K. L. Brower, Phys. Rev. B 38 (1988) pp. 9657–9666

[166] A. Stesmans and G. van Gorp, Physica B 170 (1991) pp. 507–512

[167] Y. Nishi, Jpn. J. Appl. Phys. 10 (1971) pp. 52–62

[168] P. J. Caplan, E. H. Poindexter, B. E. Deal and R. R. Razouk, J. Appl. Phys. 50 (1979) pp. 5847–5854

[169] K. L. Brower, Appl. Phys. Lett. 43 (1983) pp. 1111–1113

[170] W. E. Carlos, Appl. Phys. Lett. 50 (1987) pp. 1450–1452

[171] K. L. Brower, Phys. Rev. B 42 (1990) pp. 3444–3453

[172] J. H. Stathis and E. Cartier, Phys. Rev. Lett. 72 (1994) pp. 2745–2748
[173] A. Stesmans, Solid State Commun. 97 (1996) pp. 255–259
[174] V. Ya. Bratus', S. S. Ishchenko, S. M. Okulov, I. P. Vorona, H. J. von Bardeleben and M. Schoisswohl, Phys. Rev. B 50 (1994) pp. 15449–15452
[175] V. Ya. Bratus', S. S. Ishchenko, S. M. Okulov, I. P. Vorona and H. J. von Bardeleben, Mater. Sci. Forum 196–201 (1995) pp. 529–534
[176] E. H. Poindexter, P. J. Caplan, B. E. Deal and R. R. Razouk, J. Appl. Phys. 52 (1981) pp. 879–884
[177] P. Stallinga, T. Gregorkiewicz, C. A. J. Ammerlaan and Yu. V. Gorelkinskii, Phys. Rev. Lett. 71 (1993) pp. 117–120
[178] G. D. Watkins and J. W. Corbett, Phys. Rev. 138 (1965) pp. A543–A555
[179] M. Nisenoff and H. Y. Fan, Phys. Rev. 128 (1962) pp. 1605–1613
[180] G. D. Watkins, Radiation Damage in Semiconductors (Dunod, Paris, 1964) pp. 97–113
[181] P. Stallinga, T. Gregorkiewicz, C. A. J. Ammerlaan and Yu. V. Gorelkinskii, Mater. Sci. Forum 143–147 (1994) pp. 853–860
[182] V. A. Gordeev, Yu. V. Gorelkinskii, R. F. Konopleva, N. N. Nevinnyi, Yu. V. Obukhov, and V. G. Firsov, Preprint 1340, Leningrad Nuclear Physics Institute, Academy of Sciences of the USSR (1987), pp. 1–30
[183] R. B. Gel'fand, V. A. Gordeev, Yu. V. Gorelkinskii, R. F. Konopleva, S. A. Kuten', A. V. Mudryi, N. N. Nevinnyi, Yu. V. Obukhov, V. I. Rapoport, A. G. Ul'yashin and V. G. Firsov, Sov. Phys. – Solid State 31 (1989) 1376–1381 [Fiz. Tverd. Tela 31 (1989) pp. 176–185]
[184] V. A. Gordeev, R. F. Konopleva, V. G. Firsov, Yu. V. Obukhov, Yu. V. Gorelkinskii and N. N. Nevinnyi, Hyperfine Interact. 60 (1990) pp. 717–722
[185] G. D. Watkins, Semicond. Sci. Technol. 6 (1991) pp. B111–B120
[186] K. W. Blazey, J. A. Brown, D. W. Cooke, S. A. Dodds, T. L. Estle, R. H. Heffner, M. Leon and D. A. Vanderwater, Phys. Rev. B 23 (1981) pp. 5316–5321
[187] N. N. Nevinnyi and Yu. V. Gorelkinskii, Proc. 7th Int. Conf. on Ion Implantation in Semiconductors and Other Materials, Vilnius, 1983, pp. 61–62
[188] P. Stallinga, P. Johannesen, B. Bech Nielsen, K. Bonde Nielsen and J. R. Byberg, The Physics of Semiconductors (World Scientific, Singapore, 1996) pp. 2589–2592
[189] P. Johannesen, J. R. Byberg, B. Bech Nielsen, P. Stallinga and K. Bonde Nielsen, Mater. Sci. Forum 258–263 (1997) pp. 515–520
[190] B. Pivac, B. Rakvin, F. Corni, R. Tonini and G. Ottaviani, Defects in Electronic Materials II (Materials Research Society, Pittsburgh, 1997) pp. 293–298
[191] D. A. van Wezep, T. Gregorkiewicz, H. H. P. Th. Bekman and C. A. J. Ammerlaan, Mater. Sci. Forum 10–12 (1986) pp. 1009–1014
[192] C. A. J. Ammerlaan, H. H. P. Th. Bekman and T. Gregorkiewicz, Defects in Crystals (World Scientific, Singapore, 1988) pp. 239–261

[193] H. H. P. Th. Bekman, T. Gregorkiewicz and C. A. J. Ammerlaan, Mater. Sci. Forum 38–41 (1989) pp. 601–605

[194] T. Gregorkiewicz, H. H. P. Th. Bekman and C. A. J. Ammerlaan, Acta Phys. Pol. A 75 (1989) pp. 89–100

[195] J. Michel, N. Meilwes and J.–M. Spaeth, Mater. Sci. Forum 38–41 (1989) pp. 607–611

[196] J. Michel, N. Meilwes, J. R. Niklas and J.–M. Spaeth, Shallow Impurities in Semiconductors 1988 (Institute of Physics, Bristol, 1989) pp. 201–210

[197] N. Meilwes, J.–M. Spaeth, W. Götz and G. Pensl, Semicond. Sci. Technol. 9 (1994) pp. 1623–1632

[198] C. A. J. Ammerlaan, Yu. V. Martynov, I. S. Zevenbergen and T. Gregorkiewicz, Proc. 2nd Int. Workshop on Materials Science (ITIMS, Hanoi, 1995) pp. 654–659

[199] T. Gregorkiewicz, I. S. Zevenbergen, Yu. V. Martynov and C. A. J. Ammerlaan, Acta Phys. Pol. A 88 (1995) pp. 735–738

[200] Yu. V. Martynov, I. S. Zevenbergen, T. Gregorkiewicz and C. A. J. Ammerlaan, Solid State Phenom. 47–48 (1996) pp. 267–274

[201] H. H. P. Th. Bekman, T. Gregorkiewicz and C. A. J. Ammerlaan, Phys. Rev. Lett. 61 (1988) pp. 227–230

[202] T. Gregorkiewicz and H. H. P. Th. Bekman, Mater. Sci. Eng. B4 (1989) pp. 291–297

[203] T. Gregorkiewicz, H. H. P. Th. Bekman and C. A. J. Ammerlaan, Mater. Sci. Forum 38–41 (1989) pp. 595–599

[204] T. Gregorkiewicz, H. H. P. Th. Bekman and C. A. J. Ammerlaan, Phys. Rev. B 41 (1990) pp. 12628–12636

[205] N. Meilwes, J. R. Niklas and J.–M. Spaeth, Mater. Sci. Forum 65–66 (1990) pp. 247–252

[206] A. Hara and A. Ohsawa, Appl. Phys. Lett. 59 (1991) pp. 1890–1892

[207] C. A. J. Ammerlaan, S. J. C. H. M. van Gisbergen, N. T. Son and T. Gregorkiewicz, Nucl. Instrum. Methods Phys. Res. B 63 (1992) pp. 154–162

[208] T. Gregorkiewicz, W. Knap, H. H. P. Th. Bekman, L. C. Brunel, C. A. J. Ammerlaan and G. Martinez, Physica B 177 (1992) pp. 476–480

[209] T. Gregorkiewicz, H. H. P. Th. Bekman, C. A. J. Ammerlaan, W. Knap, L. C. Brunel and G. Martinez, Mater. Sci. Forum 117–118 (1993) pp. 521–522

[210] N. Meilwes, J.–M. Spaeth, V. V. Emtsev, G. A. Oganesyan, W. Götz and G. Pensl, Mater. Sci. Forum 143–147 (1994) pp. 141–145

[211] N. Meilwes, J.–M. Spaeth, V. V. Emtsev and G. A. Oganesyan, Semicond. Sci. Technol. 9 (1994) pp. 1346–1353

[212] M. Stavola, Early Stages of Oxygen Precipitation in Silicon (Kluwer, Dordrecht, 1996) pp. 223–242

[213] T. Mchedlidze and K. Matsumoto, J. Appl. Phys. 83 (1998) pp. 4042–4048

[214] I. S. Zevenbergen, T. Gregorkiewicz and C. A. J. Ammerlaan, Mater. Sci. Forum 196–201 (1995) pp. 855–859

[215] C. A. J. Ammerlaan, I. S. Zevenbergen and T. Gregorkiewicz, Physics of Semiconductor Devices (Narosa Publishing House, New Delhi, 1998) pp. 531–538
[216] C. A. J. Ammerlaan and P. T. Huy, Solid State Phenom. 69–70 (1999) pp. 583–588
[217] P. T. Huy, C. A. J. Ammerlaan, T. Gregorkiewicz and D. T. Don, Trends in Materials Science and Technology (Hanoi National University Publishing House, Hanoi, 1999), pp. 52–55
[218] P. T. Huy, C. A. J. Ammerlaan and T. Gregorkiewicz, Physica B 273–274 (1999) pp. 239–242
[219] M. Höhne, U. Juda, Yu. V. Martynov, T. Gregorkiewicz, C. A. J. Ammerlaan and L. S. Vlasenko, Mater. Sci. Forum 143–147 (1994) pp. 1659–1663
[220] P. M. Williams, G. D. Watkins, S. Uftring and M. Stavola, Mater. Sci. Forum 143–147 (1994) pp. 891–895
[221] Yu. V. Gorelkinskii, B. N. Mukashev and Kh. A. Abdullin, Mater. Sci. Forum 258–263 (1997) pp. 1777–1782
[222] K. L. Brower, Appl. Phys. Lett. 53 (1988) pp. 508–510
[223] K. L. Brower and S. M. Myers, Appl. Phys. Lett. 57 (1990) pp. 162–164
[224] A. Stesmans, Appl. Phys. Lett. 68 (1996) pp. 2723–2725
[225] A. Stesmans and B. Nouwen, Mater. Sci. Eng. B 58 (1999) pp. 52–55
[226] A. Stesmans and V. V. Afanas'ev, Mater. Sci. Eng. B 58 (1999) pp. 71–75
[227] K. L. Brower, S. M. Myers, A. H. Edwards, N. M. Johnson, Ch. G. Van de Walle and E. H. Poindexter, Phys. Rev. Lett. 73 (1994) p. 1456
[228] P. Stallinga, T. Gregorkiewicz and C. A. J. Ammerlaan, Phys. Rev. Lett. 73 (1994) p. 1457
[229] P. Stallinga, T. Gregorkiewicz and C. A. J. Ammerlaan, Diagnostic Techniques for Semiconductors Materials Processing (Materials Research Society, Pittsburgh, 1994) pp. 385–390
[230] P. Stallinga, T. Gregorkiewicz and C. A. J. Ammerlaan, The Physics of Semiconductors (World Scientific, Singapore, 1995) pp. 2235–2238